Development of a geostatic model for a geoscience field research station in Alberta

Jessica M. Dongas and Don C. Lawton

ABSTRACT

In taking action to mitigate greenhouse gases emitted into the atmosphere primarily from fossil fuel sources, carbon capture and storage is a method of sequestration to reduce CO_2 emissions. The geoscience field research station will serve as a research development site of advanced technologies for monitoring subsurface fluid flow. A 5 km^2 geostatic property model of effective porosity and permeability was constructed for both the shallow primary and deeper secondary injection interval at approximately 290 m and 480 m depths, respectively. The model incorporates existing wireline data from 75 wells and was populated using a Gaussian Random Function Simulation algorithm. The effective porosities of the primary and secondary injection intervals range from 0-27% and 0-18%, respectively. The primary seal interval consists of silty-sands, shales, and impermeable coal layers. The secondary seal interval consists of calcareous mudstones with bentonite layers and high illite content. The 5 km^2 x 5 km^2 property model was updated using two 3-D seismic reflection volumes and existing sonic log data. A time-depth relationship was configured by completing 8 well-ties. Velocity modeling was completed for depth domain conversion. Both injection intervals appear to be promising injection sites for CO_2 and have since been assessed for risk. A clipped 1 km^2 area of the geostatic model will be tested further using Eclipse in Petrel™ 2014.1 for computerized fluid injection simulation to study the behaviour of the CO_2 in the subsurface.

Carbon Management

Carbon capture and storage (CCS) is a method of sequestration acting to reduce CO_2 concentrations. The process consists of CO_2 capture, transport, and long-term isolated subsurface storage that is injected typically in a supercritical phase (IPCC, 2005; Alshuhail, 2011). For successful sequestration, the formation must have the capacity to store the CO_2, which is dependent on the porosity, permeability, pressure, depth, and temperature of the formation (IPCC, 2005). The pressures used for injection must not exceed caprock failure pressures, as this will lead to induced fracturing to not only the target interval, but potentially to the impermeable seal above (Alshuhail, 2011; Bachu, 2002). To ensure proper confinement and isolation of the CO_2, there must be a seal or a set of impermeable layers above the target interval to prevent mobility and leakage.

There are two types of sites for the interest of sequestration, these include saline-water (brine) formations and depleted hydrocarbon (HC) reservoirs (Hovorka et al., 2008). With CCS in depleted HC reservoirs, the geometry of the reservoir, seal integrity, and physical trapping mechanism are known (Lawton, 2014) due to previous investigation prior to production. The injection of CO_2 has also been used for enhanced oil recovery (EOR), by reversing the trends of pressure decline, acting on the miscibility of CO_2 and oil to increase the volume and decrease the viscosity of the remaining oil to increase mobility (Hovorka et al., 2008). One risk subject to this type of site is the potential leakage through abandoned wells. With CCS in deep brine formations, there are multiple seals that may overlay the interval to prevent vertical movement of the plume, with few wells penetrating the formation to cause leakage pathways (Lawton, 2013). The main trapping mechanism with this site type is solubility, which may pose risks if the reservoir itself is not geometrically confined, especially since there is typically little knowledge on the integrity of the seal (Lawton, 2013) due to the lack of exploration.

In taking action to mitigate Greenhouse Gases (GHG) emitted into the atmosphere primarily from fossil fuel sources, many companies within the oil and gas industry are taking social responsibility and funding research to inspect the potential for long-term storage of CO_2 in nearby subsurface geological formations (Smyth et al., 2011). The proposed Geoscience Field Research Station (GFRS) comprises efforts from Cenovus Energy, Carbon Management Canada (CMC), and the Consortium of Elastic Wave Exploration Seismology (CREWES) at the University of Calgary.

Location

The study area is within the province of Alberta, located 188.9 km southeast of Calgary (Figure 1) in Section 22, Township 17 and Range 16 west of the 4th Meridian.

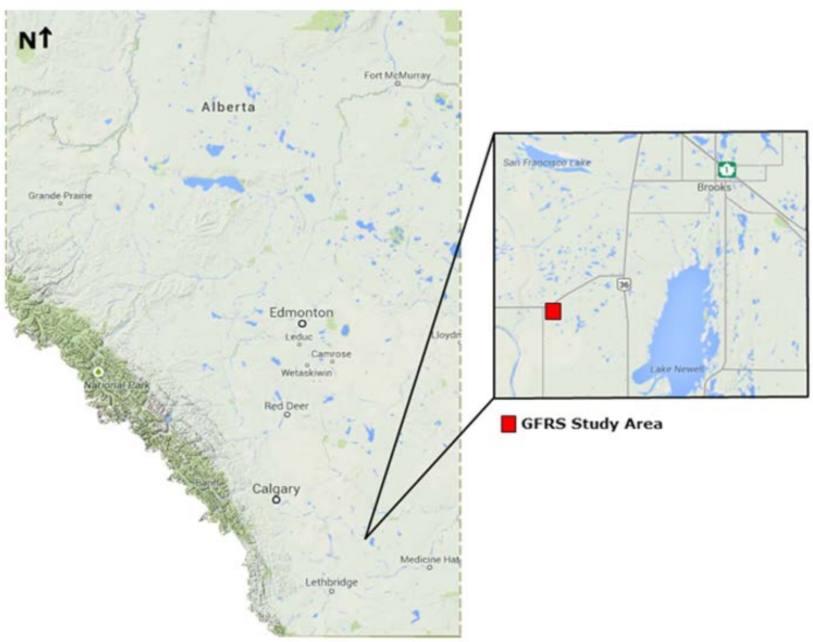

FIG. 1. Location of the GFRS study area in Alberta (© Google, INEGI 2014).

The main vertical well in the area (7-22-17-16W4) was used for petrophysical analyses and knowledge regarding the depth of the target intervals is located at the margin of the GFRS site.

Geological Background

Shetson (1987) mapped the surficial geology of the area and determined that the sediments about the GFRS study region are composed of till of uneven thickness, with 30 m of locally water-sorted material. Determined to be stagnation moraine, these glacial melt-out sediments were reworked by fluvial and eolian processes causing the undulating to hummocky topography as a function of the till thickness. Following the topography of Newell County, the unconsolidated materials are thickest in the NW and SE. The volume of clay within the glacial sediments affect the permeability, causing slower rates of groundwater recharge through precipitation and infiltration of any contaminants in the area. (WorleyParsons Komex, 2008; Shetson, 1987)

During Late Campanian time, Southern Alberta was located at approximately 55N paleoaltitude situated in a warm, humid, temperate to subtropical climatic setting (Hamblin and Abrahamson, 1996). The Montana Group/Belly River Group (Table 1) was deposited during this time and is composed of the Bearpaw, Oldman, and Foremost formations. The Oldman Formation was primarily deposited in a transgressive environment, and is composed of two divisible parts that include the Lethbridge Member and Comrey Member (Russell and Landes, 1940; Hamblin, 1997). The Lethbridge Member consists of mudstone-dominated strata with carbonaceous sandstones and shales, with bentonitic beds and the Lethbridge Coal Zone near the top (NRCAN, 2014) of the formation. The lower Comrey Member consists of lenticular fining-upward sandstone filled fluvial channels, remaining relatively continuous with a thickness of 15 m near the base (Hamblin, 1997). The fresh water light-grey cross-bedded sandstones are generally very weakly cemented and form the commonly known topography of the Alberta Badlands (NRCAN, 2014).

Table 1. The major hydrogeological units in the stratigraphic column for the Newell County region, modified from WorleyParsons Komex (2008).

Formation		Member	Dominant Lithology	Aquifer/A quitard	Thickn ess (m)
Overburden			Clay, Till, Silt, Sand, Gravel	Both	1-120
		Sand, Gravel	Sand, Gravel	Aquifer	0-40
Horseshoe Canyon			Sandstone, Siltstone, Coal	Aquifer	<80
Bearpaw			Shale	Aquitard	<140
Belly River Group	Oldman	Lethbridge	Coal	Aquifer	<20
Belly River Group	Oldman	Dinosaur Park	Sandstone, Siltstone, Mudstone	Aquifer	<50
Belly River Group	Oldman	Siltstone	Siltstone, Shale, minor Sandstone	Aquitard	<20
Belly River Group	Oldman	Comrey	Sandstone, Siltstone	Aquifer	<20
Belly River Group	Foremost	Taber	Coal	Aquifer	<15
Belly River Group	Foremost		Siltstone, Shale, some Sandstone	Aquifer	<110
Belly River Group	Foremost	McKay	Coal	Aquifer	35
Belly River Group	Foremost	Basal Belly River	Sandstone	Aquifer	20

This study used different geological nomenclature than that used typically in academia and industry, thus for stratigraphic reference the outline for the primary and secondary injection zones and seals can be seen in Table 2.

Table 2. Stratigraphic column outlining past and current nomenclature used for the GFRS model.

McNeil and Caldwell (1981) *Webb et al. (2005)** *Nielsen and Schröder-Adams (1999)*** *Leckie and Smith (1992) ****				THIS STUDY *After Nielsen et al. (2003), Leckie et al. (2004), and Christoper et al. (2006)*			Well Tops Used	General Lithology	Reservoirs & Seals
PERIOD	STAGE / AGE (Ma)	SEDIMENTARY CYCLES		ALBERTA SOUTHERN PLAINS			ALBERTA SOUTHERN PLAINS		
LATE CRETACEOUS	CAMPANIAN	NIOBRARA MARINE CYCLOTHEM	REGRESSION	MONTANA GROUP	BEARPAW FORMATION		BEARPAW		
					OLDMAN FORMATION		OLDMAN		
					FOREMOST FORMATION		FOREMOST		Seal
							BASAL BELLY RIVER SST		Primary Injection
				PAKOWKI FORMATION			PAKOWKI		
	84			MILK RIVER FORMATION			MILK RIVER		
	SANTONIAN		TRANSGRESSION	COLORADO GROUP	NIOBRARA FORMATION	FIRST WHITE SPECKS MEMBER	COLORADO		Seal
	87					MEDICINE HAT MEMBER	MEDICINE HAT		Secondary Injection
	CONIACIAN					VERGER MEMBER	**BASE MEDICINE HAT**		
	89	GREENHORN CYCLOTHEM	REGRESSION			***BENTONITE MARKER***			
	TURONIAN 93				CARLILE FORMATION				
	CENOMANIAN		TRANSGRESSION		SECOND WHITE SPECKS FORMATION		**SECOND WHITE SPECKS**		
					BELLE FOURCHE FORMATION				
	97-99				FISH SCALES FORMATION				
	ALBIAN				WESTGATE FORMATION		BASE FISH SCALES		
			REGRESS**		BOW ISLAND FORMATION		BOW ISLAND		
			TRANS*		JOLI FOU FORMATION		JOLI FOU		
			REGRESS***	MANNVILLE GROUP			MANNVILLE		

Summary of Target and Seal Intervals

The summary of the target and seal intervals are described in the respective order of deposition.

Medicine Hat Member

The second target of interest is located within the Medicine Hat Member at approximately 480 m depth and occurs below the First White Specks Member in the Colorado Group. The formation consists of at least three upward-coarsening very fine-grained sandstone and siltstone units that was deposited in a shallow marine shelf environment during the Santonian stage (Leckie et al., 2013).

These units are a heterogeneous mix of thinly bedded, very-fine to fine-grained sandstone and coarse siltstone beds (Schroder-Adams et al., 1997) that combine to give a total thickness of up to 60 m, and individually range from 3-11 m (Leckie et al., 2013). The coarser sand and bioclastic materials are most commonly present at the top of the sand bodies, which gives each coarsening upward sandstone unit a sharp contact at the top and a gradational base (Schroder-Adams et al., 1997). The sandstone units are described to be compositionally mature litharenites that are graded, calcareous, and are mottled as a result of the bioturbation and vertical burrows recognized by the Skolithos Ichnofacies (Schroder-Adams et al., 1997).

The Medicine Hat Member as a whole was modeled to predict an effective porosity range of 3-18% and a permeability ranging from 0-1 mD. These values predicted by the geostatic model which used a Gaussian random function simulation algorithm to populate the cells was comparative to the values published by Schroder-Adams et al. (1997) which gave a porosity range of 10-14% and permeability that generally is less than 1 mD.

First White Specks Member

The First White Specks (1WS) Member is a calcareous mudstone that overlies the Medicine Hat Member of the Niobrara Formation, within the Colorado Group. In this project, the 1WS Member is referenced to the Colorado Formation. The deposition of the 1WS Member is the resultant of the maximum extension of the Interior Seaway, which occurred during the Late Santonian as a part of the Niobrara Cycle (Nielsen et al., 2008).

The 1WS Member has a thickness that ranges from 20 - 80 m, thins eastward (Nielsen et al., 2008), and contains dark gray shales that are fissile to platy in nature (Nielsen et al., 2003). The presence of thin bentonite (0.5 – 3 cm) (Nielsen et al., 2003) layers results in high uranium content and is shown in the spectral gamma ray curves (Leckie et al., 2012). The lack of bioturbation in comparison to the overlying Milk River Formation and underlying Medicine Hat Member (Nielsen et al., 2003) describes a disoxic environment, where low oxygen levels were present during the time of deposition (Nielsen et al., 2012). The abundant laminae of fecal pellets rich in nanofossils, numerous bentonites, and low-angled beds depict the palaeoenvironment which had a low energy regime in a lower offshore to shelf setting (Nielsen et al., 2008).

Publications addressing the rock properties of the Upper Colorado mudstones in the plains of southern Alberta are sparse (Nielsen et al., 2003). However, a study located northeast of the Bow Island Arch extension of the Sweetgrass Arch was completed by Taylor (2011) gave insight to the seal capabilities as a result of the porosity and permeability ranges. This study overlies the southern Alberta-Saskatchewan border, which is further southeast of the GFRS area.

Samples from the 1WS Member gave a bimodal porosity distribution, indicating that within each sample there are significant volumes of clast sizes within the sediment ranging from clay, silt, and sand (Taylor, 2011). Illite clays are abundant in the Upper Colorado Group (Taylor, 2011), which act as a significant contributor to the total porosity average of 19.76%, as clay particles have higher surface area and are bound with water (Robinson, 2008). The average permeability measured by mercury injection at 471.6 m depth was 151 nD, and gave a mean pore throat radius of 35.0 nm (Taylor, 2011). However, the study examined another data set that gave a permeability range of 0.1-10 mD from point probe measurements (Taylor, 2011). The Colorado Formation (1WS Member) was modeled to predict a range of 0-14% effective porosity and permeability range of 0-1 mD. These values were predicted by the geostatic model, which used a Gaussian random function simulation algorithm and are comparative to the point probe permeability measurements examined by Taylor (2011). The significant volumes of clay and mud within the 1WS Member will act as an effective barrier overlying the Medicine Hat Member, as it will create a laterally extensive impermeable barrier (Taylor, 2011) – which is a key element in finding a seal that will successfully inhibit vertical migration of CO_2 towards the surface. However, abundant clay minerals in subsurface formations can propose other challenges due to the increased fluid sensitivity and can affect drilling and completion operations.

Basal Belly River Sandstone

The shallow target is described to be a regressional shoreline sandstone (Hamblin and Abrahamson, 1996) characterized to be the basal unit of the Foremost Formation, an interval of strata deposited during the Late Cretaceous within the Western Canada Sedimentary Basin (WCSB) in the Montana Group at approximately 290-310 m depth. The reservoir was interpreted to reach a maximum thickness of 12.5 m in the GFRS study area. Within Newell County, the Foremost Formation (including the BBRS) was interpreted to have a thickness up to 238 m, which is comparable to that of the measured thickness of 225 m given by WorleyParsons Komex (2008).

The reservoir is described as a fine- to medium-grained sandstone that has poorly to well-sorted, angular to sub-angular grains that are loosely packed with calcite cement pore-fill. Large crystals of diagenetic calcite cement make up to 40% of the rock, and diagenetic clay makes up to 20% of the rock. The diagenetic clay consists of kaolinite (10%), chlorite (5%), and the remaining 5% includes volumes of illite, montmorillonite, and smectite. The sandstones permeability is affected by the abundant clay-rich horizons and discrete calcite cemented horizons acting to create vertical and lateral flow barriers. Drilling through the BBRS often damages the sandstone due to its under-pressured condition and abundant clay content, as the kaolinite acts to block pore throats under high pressure fresh-water drilling systems and acid treatments can cause iron oxide gels to produce from the chlorite content. (Hamblin and Abrahamson, 1996)

The BBRS is assumed to have a range of 0-27% effective porosity and permeability range of 0-300 mD. These values were predicted by the geostatic model which used a Gaussian random function simulation algorithm and are comparative to the values published by Hamblin and Abrahamson (1993) which gave a porosity range of 10-24% and permeability ranging from 8 mD to 45 mD in related channel sandstones.

Foremost Formation

The Foremost Formation is composed of interbedded sandstone, siltstone, and two coal zones – all of which represent transgressive and regressive cycles (Hamblin and Abrahamson, 1996). The Taber Coal Zone is located at the top and the McKay Coal Zone is located at the base of the formation (NRCAN, 2014). The overlying members of the Foremost Formation act as a seal to the bottom-most N-S oriented Basal Belly River Sandstone (BBRS), which is located below the McKay Coal Zone (WorleyParsons Komex, 2008). For the purpose of this study, the Foremost Formation and the BBRS unit were separated to conduct reservoir property modeling and evaluation.

The Foremost Formation has a range of 0-28% effective porosity and permeability range of 0-360 mD. These values were predicted by the geostatic model, which used a Gaussian random function simulation algorithm. The interbedded siltstones, coal, and shales within the Foremost Formation act as a laterally extensive seal to prevent vertical migration of injected CO_2, as the relative permeability with respect to clay-bound water is very low (Pedersen, 2013).

Hydrogeological Background

One of the main risks of injecting CO_2 into shallow depths less than 1 km^2 in the subsurface is leakage through nearby abandoned wells and water wells on private properties. The addition of CO_2 into potable water can affect the pH levels, solubility, and mobility of elements of compounds that are naturally occurring and potentially increase their concentration (Trautz et al., 2012). It is important to assess the static groundwater levels and the flow direction in order to adopt a hypothesis of how the plume will behave with simulation preceding the injection. A regional groundwater assessment was conducted in Newell County, Alberta by WorleyParsons Komex Resources & Energy in August 2008. The data regarding the static water levels, as well as general structure for groundwater flow is provided in the GFRS study area and taken from the report.

The surface topography in the region of study is fairly flat, averaging around 770 m above sea level (asl) and steepens westward. The topographic divide forming the NE and SW boundaries of Newell County dominates the groundwater flow of the static water levels in the overburden sediments, Bearpaw Formation, and the Oldman Formation. As a general rule of thumb, static groundwater levels mirror the surface topography. The divide forms the nearby drainage basins of the Red Deer River and Bow River, respectively. The regional recharge areas for groundwater have also been assessed. For the interest of this project, the local recharge area is just east of the Kitsim Reservoir and Lake Newell. The GFRS region is an area of transition, and a small area of discharge has been identified to be just northwest of Highway 539. (WorleyParsons Komex, 2008)

The groundwater throughout Newell County has been characterized to be brackish, containing up to 1000-3500 mg/L Total Dissolved Solids (TDS). Hardness with respect to calcium decreases with depth, however the fluoride concentration increases with depth with values above the safe drinking limits. The groundwater vulnerability has been determined to be low in the GFRS study area, and much of the groundwater resources in Newell County are for agricultural use rather than domestic. Higher groundwater usage is found directly west of Lake Newell and south of the 7-22 well, measuring to be less than 10 m^3/day. There are no water wells that will be directly affected, and the three domestic water wells that are nearby are located 5 km west and south from the main well, which have low probability of being at risk since groundwater flow is northward in the Foremost Formation and there has been a discharge zone identified northwest of the site. A summary of subsurface formations and their respective groundwater flow can be found in Table 3 below. (WorleyParsons Komex, 2008)

Table 3. Displays the extrapolated groundwater flow directions in the subsurface based on the map of static groundwater levels. Taken from the regional groundwater assessment conducted by WorleyParsons Komex (2008).

Formation	Groundwater Flow Direction
Overburden	NE-SW
Bearpaw	NE-SW
Oldman	NE
Foremost	N

Objective

The objective of this project is to develop a geostatic model that incorporates geological and geophysical information of the GFRS area to provide a prediction as to how fluid simulation will behave in both the shallow primary and deeper secondary injection intervals. The GFRS will serve as a pilot site for researchers of all suits, and act to test cutting-edge measurement monitoring and verification (MMV) technologies for the injection and storage of 1000 tons of CO_2 injected per year. The development of this research site will not only address health, safety, and environmental concerns – but will act to testify injection and reservoir management, and the models that have only been tested virtually. Implementation of MMV technologies over the course of a CCS project is required not only by regulators, but also is needed to confirm the behaviour of the CO_2 in the subsurface, to gain acceptance by the public, as well to reduce any potential liability for the study area in the future (Spangler, 2007).

The region of study is geologically stable with flat-lying subsurface layers, with no observed fault structures. Seismic interpretation of reflection and imaging techniques have provided a means to identify and characterize the lack of any discontinuities, and an understanding of the regional behaviour of the lithology and thickness of layers that are of interest for CO_2 sequestration.

DATASETS AND SOFTWARE USED

The IHS Energy Canada databases provided the data used in the construction of the 3-D model, which was completed in Schlumberger's Petrel™ version 2014.1 licensed by the University of Calgary (Table 4). Information retrieved from these sources was provided access through Schlumberger Limited. Well locations, deviation surveys, well tops, well logs, and core data from 198 wells within a 10 km radius of the main GFRS onsite well 7-22 was obtained. For the construction of the petrophysical model, only 75 of the 198 wells were thoroughly analyzed and are found within 5 km radius of the main well. For the well-tie process, only eight wells were tied to the two 3-D seismic volumes.

Table 4. Provides a summary of the software utilized in the completed work for this project.

Software	Company	Use
AccuMap®	IHS Energy Canada	A data management and analysis software developed by IHS that enables access to multiple oil and gas databases for well location, production, and geological information for online download.
Acculogs®	IHS Energy Canada	A database that allows users to connect to the IHS Information Hub and data within Canada that is found in Accumap®. Rastered well log images, digital LAS files, production and core data, as well as deviation surveys can be downloaded from registered wells within the Western Canada Sedimentary Basin.
Petrel™ E&P Software Platform	Schlumberger Canada Limited	An advanced interpretation environment developed by Schlumberger Canada Ltd., where geological and geophysical systems merge to analyze both wireline and seismic data to delineate and characterize subsurface target volumes.

Two 3-D seismic volumes were used for interpretation of subsurface formations. A 3-D/1-C volume provided courtesy of Cenovus Energy and was collected in 1997. The newly acquired 3-D/3-C seismic volume was collected in May 2014 by Carbon Management Canada. Information on both seismic surveys can be seen in Table 5. The newly acquired volume is located within the extent of the larger 1997 3-D/1-C volume. The final 3-D volumes were processed into post-stack migrated seismic sections by Dr. H. Isaac, a researcher in part of CREWES and CMC groups, which were used for interpretation using Petrel™ E&P Software Platform 2013.3. Google Maps™ 2014 was used to generate location maps. Microsoft® PowerPoint® and Word® were used to construct and edit figures and tables.

Table 5. Lists main acquisition parameters of the two stacked migrated 3-D seismic volumes.

Type of Seismic Reflection Volume	3-D/1-C	3-D/3-C
Date	1997	2014
Company	Cenovus Energy	Carbon Management Canada
Receiver Spacing	70	10
Source Spacing	140	10
Source	Dynamite	Vibroseis
Replacement Velocity	2600 m/s	2600 m/s
Sample Interval	2 ms	2 ms
Filter	None	Bandpass 15/20-120/140

5 KM^2 GEOSTATIC PROPERTY MODEL

Interpretation of Township 17

The project has 198 wells with digital LAS files imported that include wells outside of Township 17, within a 10 km radius from the main onsite well 7-22. Few core data measurements were also used to develop relationships for the porosity and permeability calculations. Effort was focused on a total of 75 wells for formation well top interpretation, and only 17 of those wells are within a 5 km radius of the main well 7-22.

The wireline data suite is comprised of gamma ray, spontaneous potential, compressional sonic, shallow-deep resistivity, bulk density, and lastly density and neutron porosity logs. A sample of how the formation boundaries were interpreted is demonstrated in Figure 2 displaying the well section window interface in Petrel™, and the shallow target can be identified in the main well 7-22 at approximately 290 m depth.

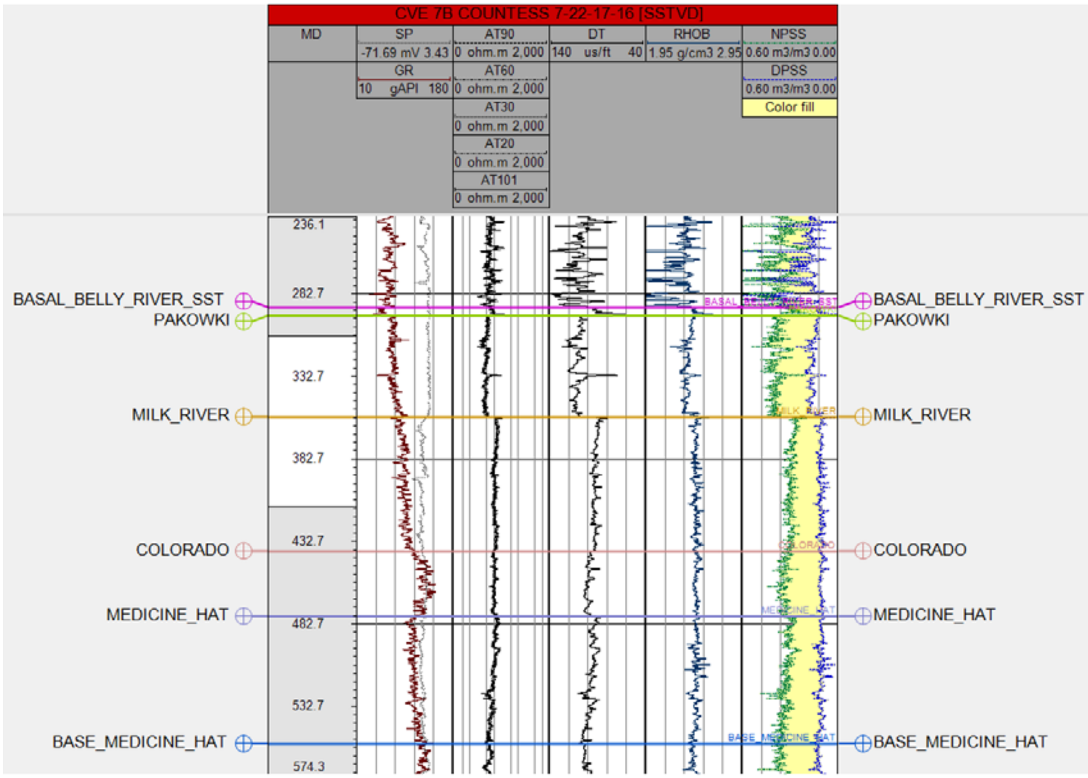

FIG. 2. Well-section window in Petrel™ displaying the wireline data available in 12-16 well. The cloud identifies the primary injection interval, the Basal Belly River sandstone.

Shallow wireline data above 290 m depth in most of the 75 main wells was unavailable, or had skewed data values as a result of being logged through casing. For the purpose of computerized simulation for CO_2 injection, the top of formations above the Basal Belly River sandstone were interpreted based on the general findings of mapped bedrock geology by Shetsen (1987). The Earth's surface was mapped by each well's Kelly Bushing (KB).

Contoured Surface Generation in Depth

Contoured surfaces that demonstrate the subsurface structure were generated through the interpolation of well locations with interpreted formation top depths. The surfaces are defined by elevation depth (m), with mean sea level as the datum (z=0) and can be seen in Figures 3-6. The surfaces expand to fill the 10 km radius from the main GFRS onsite injection well 7-22, utilizing the main interpretation completed on the 75 wells within a 5 km radius. The behaviour of the surfaces outside the 5 km radius was dependent on the interpolation of data points, as well as the imported system well top that was not adjusted. Some erratic behaviour such as surfaces crossing, pinching, or coning upward or downward was due to a poorly interpreted system well top. Individual attention was paid to these specific areas, and was controlled by identifying the well UWI attached to the poorly picked well top and was changed based on the available well data.

To minimize structural crossing and pinching of top/bottom surfaces, iso-points were computed between each using Eq – 1 (Schlumberger, 2014).

$$SURFACE_B - SURFACE_A = ISOPOINTS \qquad \text{(Eq – 1)}$$

The output isopoints item of each zone contains statistics, where the minimum and maximum thicknesses of each zone can be obtained. The maxima and minima of each formation were applied in a set of mechanical workflow equations (Zaluski, 2014) to honour the interpretation and to prevent surfaces from acting erratically. A general subset of these equations can be seen in Eq 2-5 (Zaluski, 2014).

Iso_TopSurface = Top Surface - Bottom Surface (Eq – 2)

Iso_TopSurface = IF(TopSurface<Min Thickness, Min Thickness, Thickness of TopSurface) (Eq – 3)

BottomSurface = IF(BottomSurface>TopSurface - Min Thickness, TopSurface - Min Thickness, Thickness of BottomSurface) (Eq – 4)

TopSurface = BottomSurface+Iso_TopSurface (Eq – 5)

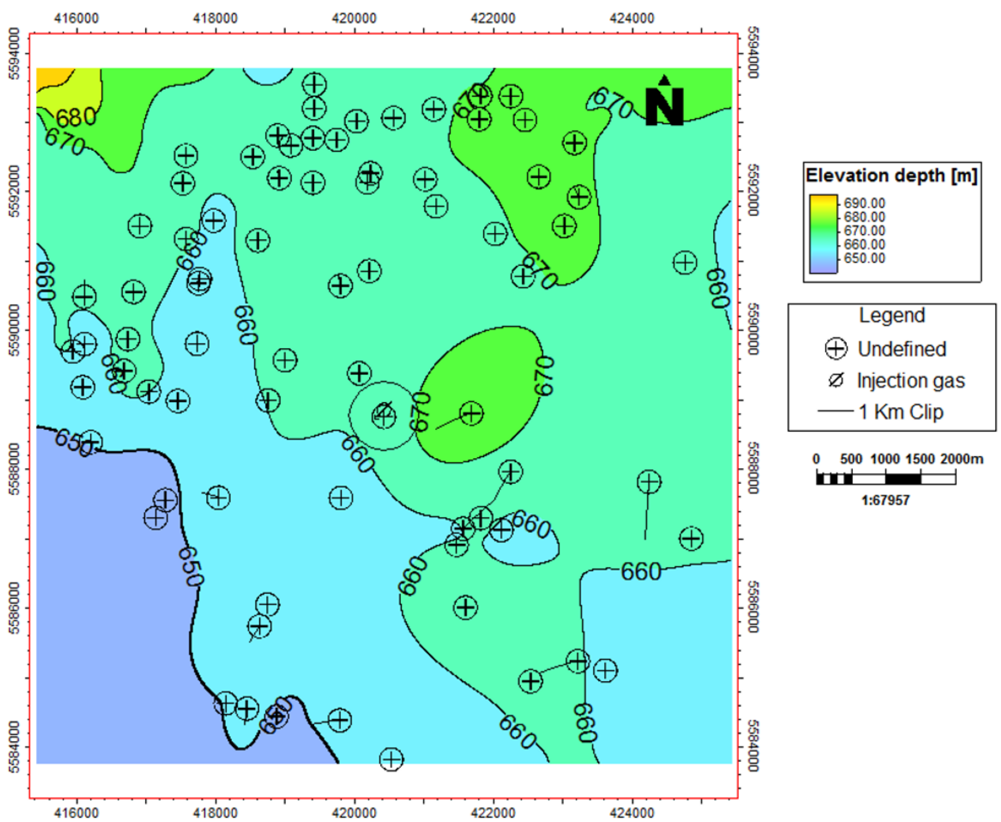

FIG. 3. Structural map contoured at 10 m intervals to the top of the Foremost Formation surface.

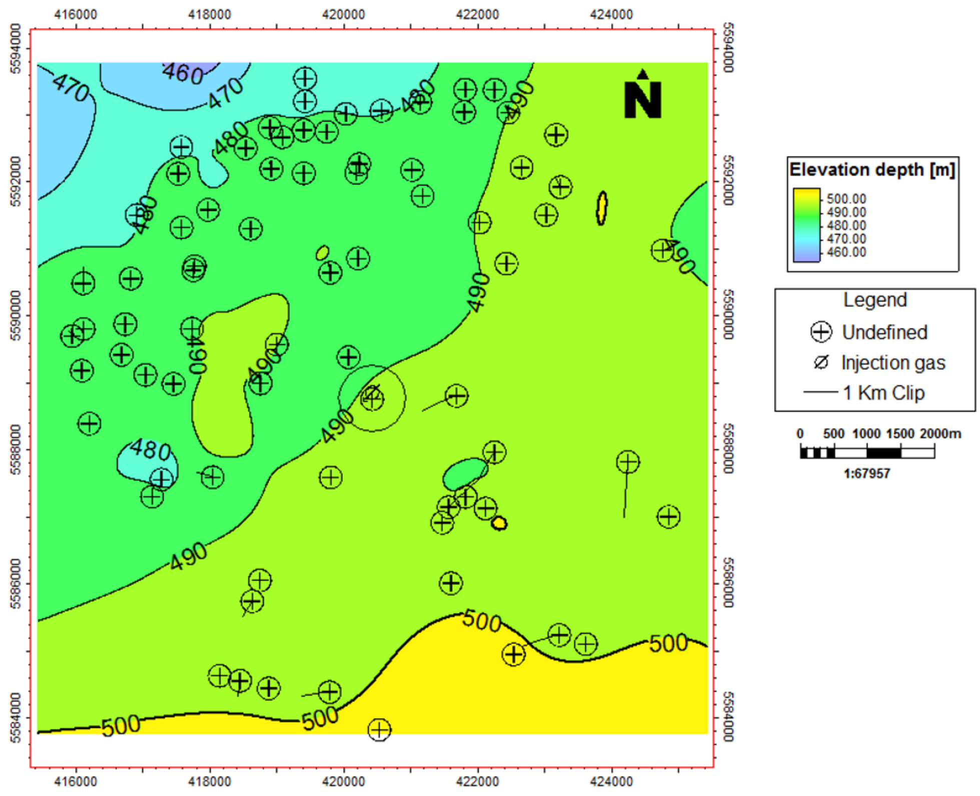

FIG. 4. Structural map contoured at 10 m intervals to the top of the BBRS surface.

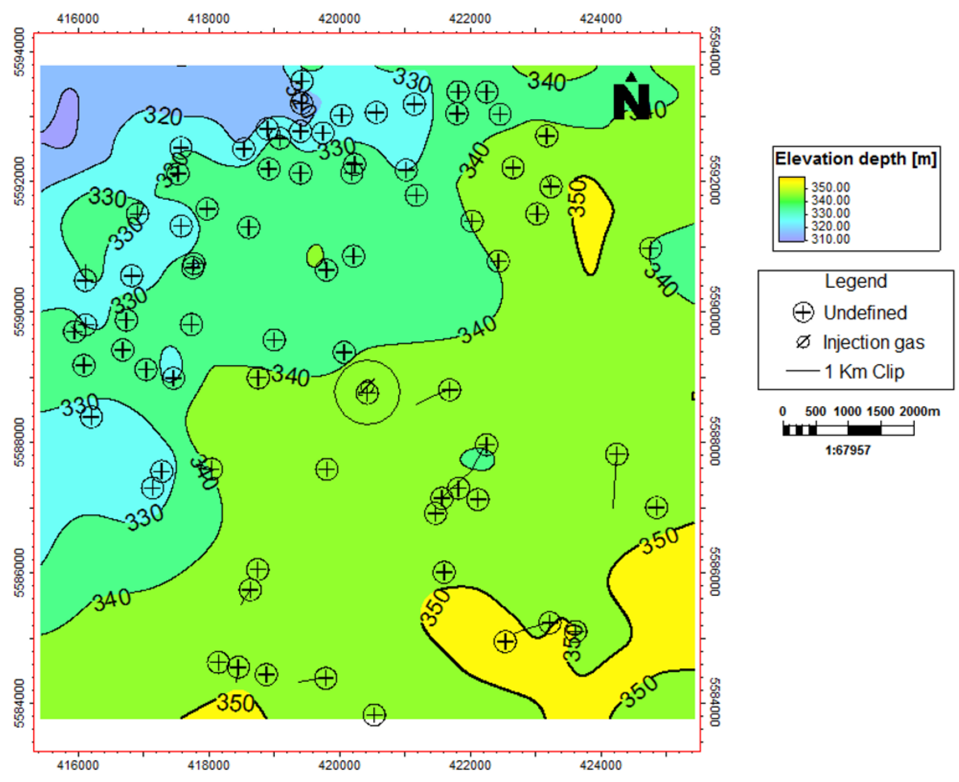

FIG. 5. Structural map contoured at 10 m intervals to the top of Colorado Formation surface.

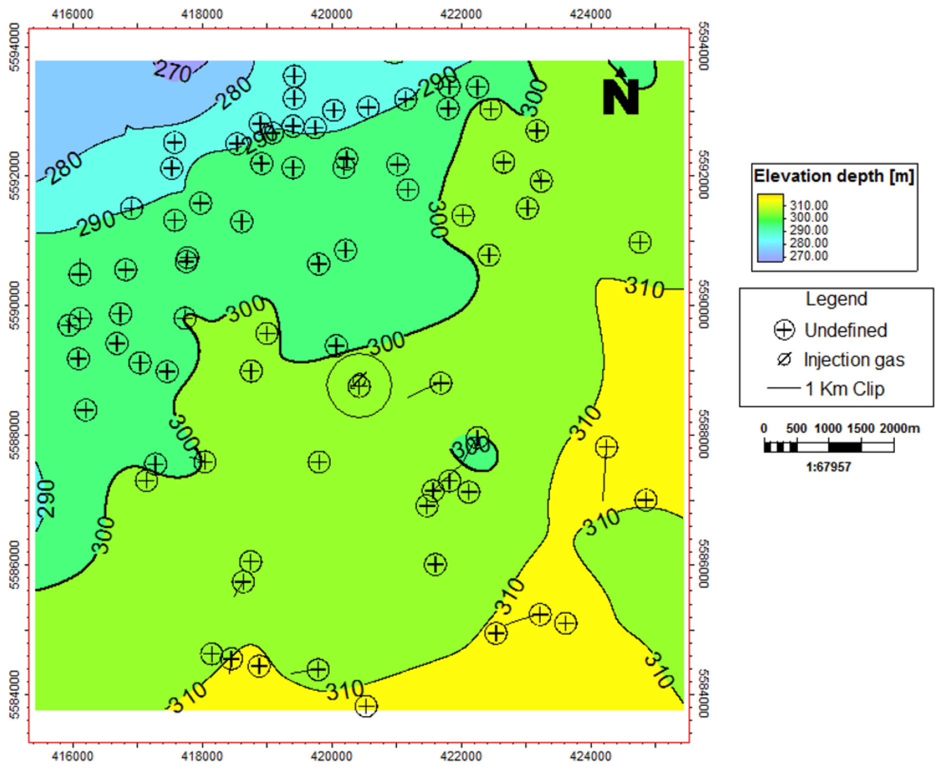

FIG. 6. Structural map contoured at 10 m intervals to the top of Medicine Hat Member surface.

Isopach Maps of Target and Seal Intervals

Isopach maps were generated for the Foremost, BBRS, Colorado, and the Medicine Hat units utilizing the iso-points that were generated for each zone to QC the data for the contoured surfaces. The difference in creating an isochron and a structural map is that the isochron is a map of contoured thickness for the specified zone. The Petrel™ interface asks for the z-thickness recalling the computed iso-points for each zone with differential ranges of maxima and minima. Whereas the structural maps are contoured to the elevation depth to which it is located in the subsurface. The isopach maps are computed in depth (m) and can be seen in Figures 7-10.

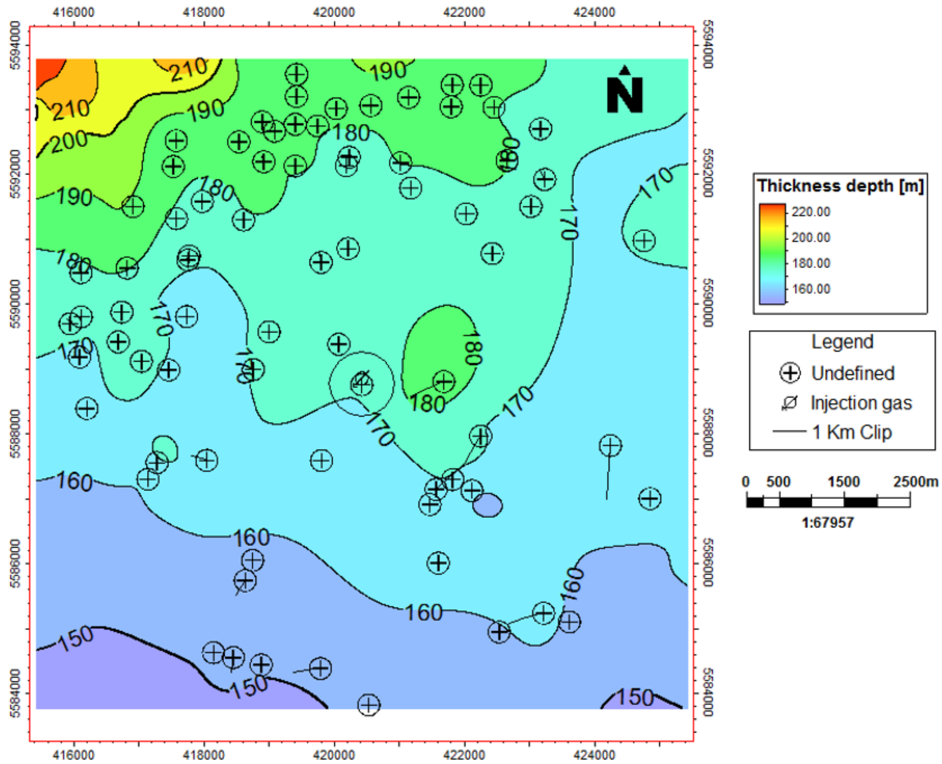

FIG. 7. Isopach map contoured at 10 m intervals of the Foremost Formation.

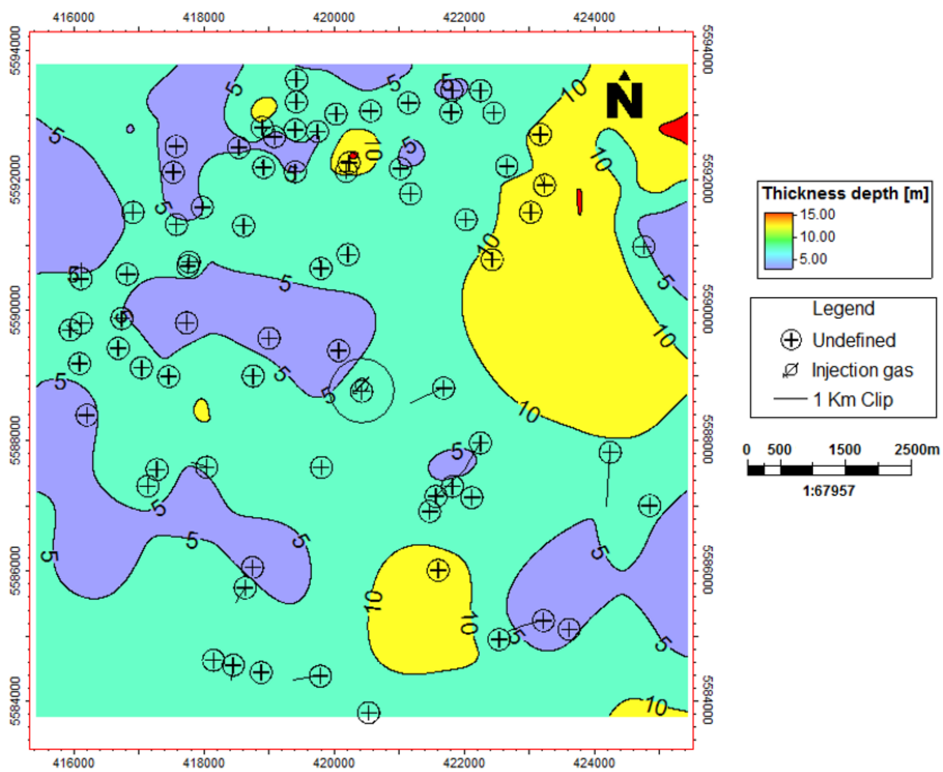

FIG. 8. Isopach map contoured at 5 m intervals of the BBRS.

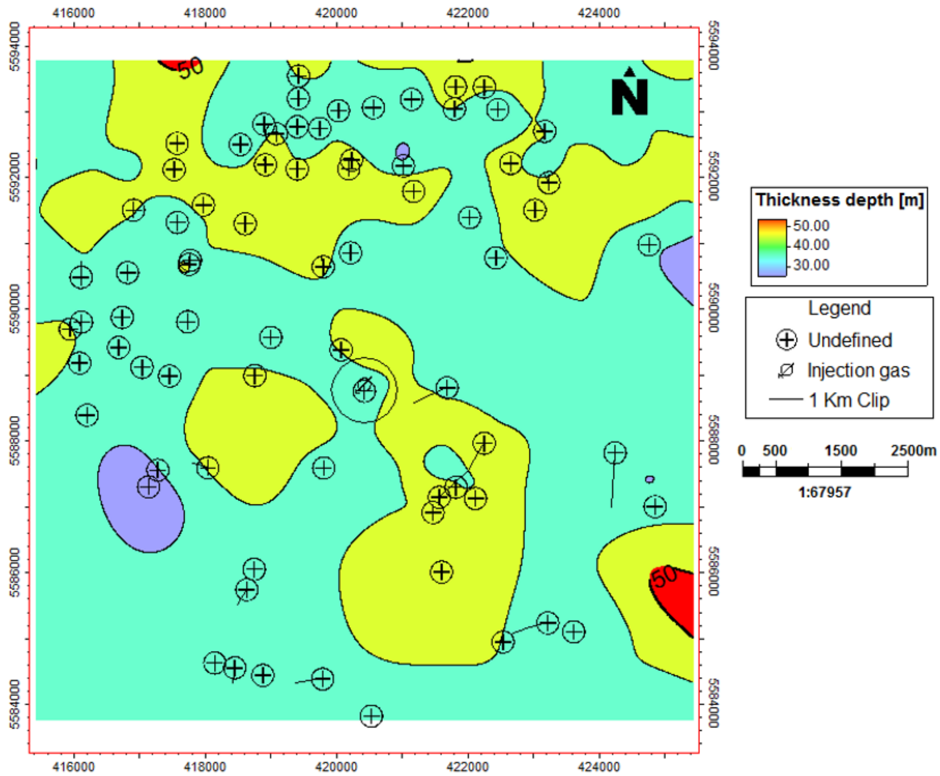

FIG. 9. Isopach map contoured at 10 m intervals of the Colorado Formation.

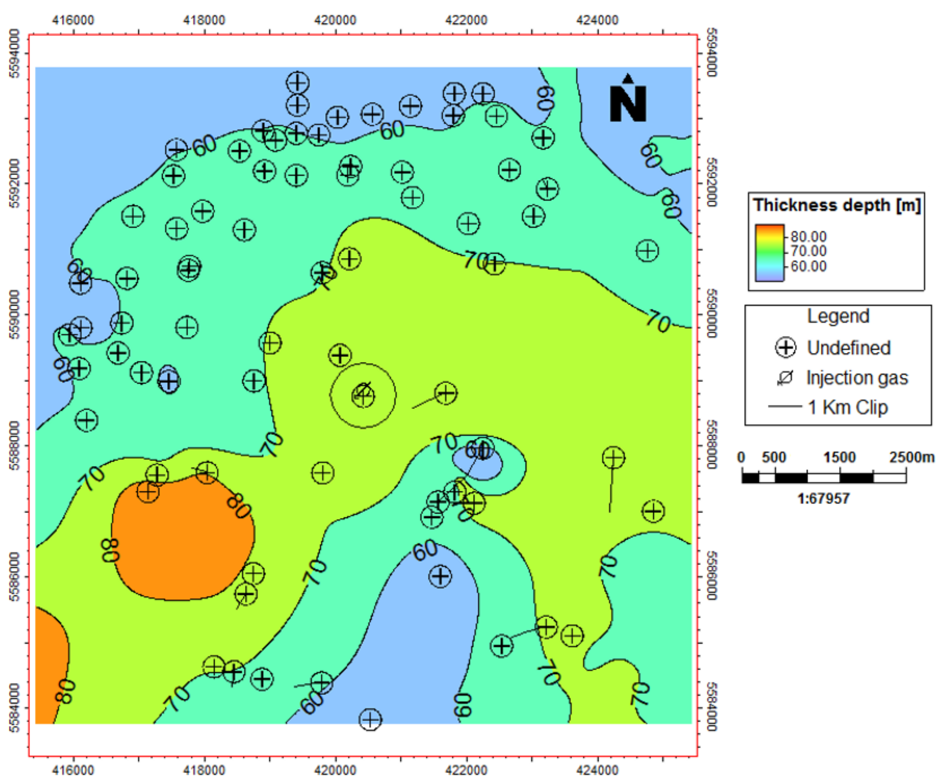

FIG. 10. Isopach map contoured at 10 m intervals of the Medicine Hat Member.

Model Geometry Definition and Gridding

The model was defined a volume of 200 x 200 x 922 (nI x nJ x nGridLayers) using a simple vertical pillar grid method, and has a total of 36 million 3-D cells. The geometry of the model is simple, reflecting the geology in the Plains and no fault model was created (Figure 11).

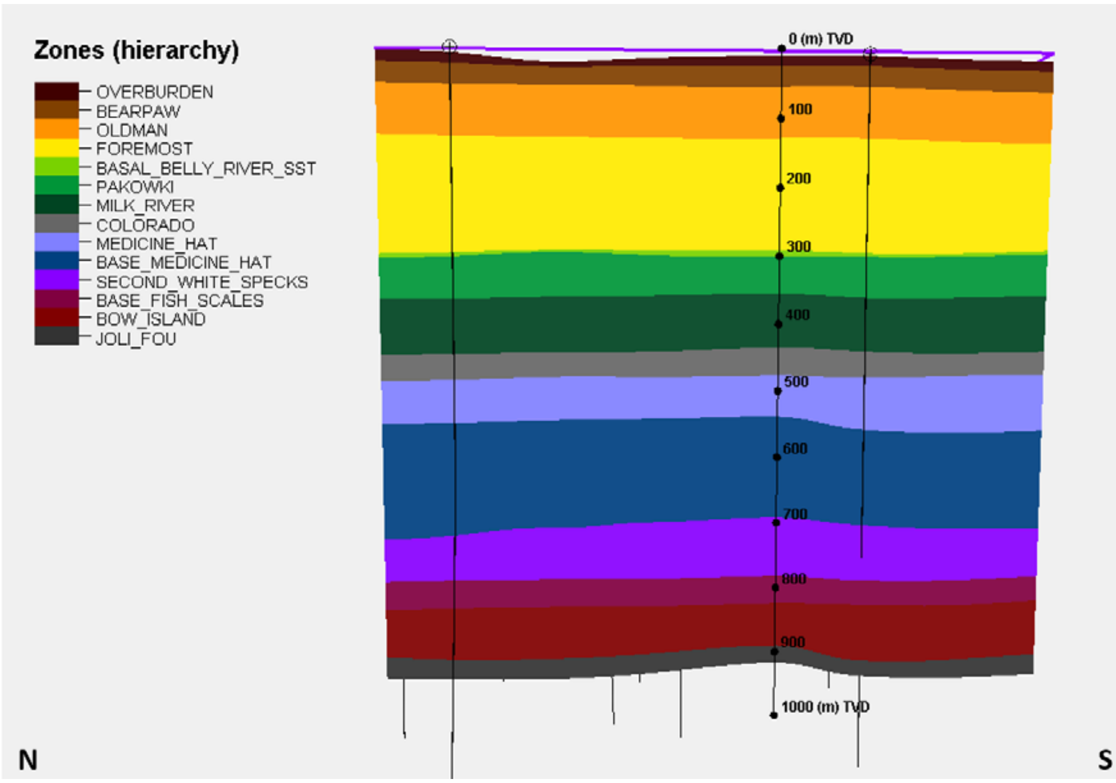

FIG. 11. Simple layer-cake geological structure of the GFRS study area, modeled by formation and shown in colours attributing to the zone hierarchy.

The horizons constructed in 3-D honour the structural framework of the previously defined surfaces in 2-D, by the interpretation and interpolation of the different formation tops. Layering of the grid cells within the model enables cell size to be defined separately for zones of high and low importance for reservoir simulation. The layering of the cells was programmed to build the cells upward, which is geologically sound to follow the underlying surface rather than to follow the topographic character of the region, to eliminate misleading artifacts in the layering of populated properties. Each layered zone was divided based on the assigned cell thickness. Cells in the seal and target intervals were assigned a height of 0.5 m, and those in non-important units were assigned a height of 5 m. In the target intervals where the simulation will take place, it was important to define a finer-scaled cell thickness in order to monitor how the plume will behave based on a well-represented property population. It will become important to identify and characterize any vertical fluid movement into the seal intervals based on the assigned petrophysical properties. In the cells of low importance, larger scaled cell thickness is appropriate because the averaged properties in these intervals will not affect the simulation and thus effort should be spent in detailing the areas greatest of concern. Table 6 lists the layered zones for each horizon with the assigned cell size for the model.

Table 6. Lists layered zones for each horizon with the assigned cell thickness size for the model. Note that the Overburden, Bearpaw, and Oldman formations were not modeled.

Formation	Layering of Zones	Cell Thickness (m)
Foremost	Follow Base Surface	0.5
Basal Belly River SST	Follow Base Surface	0.5
Pakowki	Follow Base Surface	5
Milk River	Follow Base Surface	5
Colorado	Follow Base Surface	0.5
Medicine Hat	Follow Base Surface	0.5
Base Medicine Hat	Follow Base Surface	5
Second White Specks	Follow Base Surface	5
Base Fish Scales	Follow Base Surface	5
Bow Island	Follow Base Surface	5
Joli Fou	Follow Base Surface	5

The layering of a portion in the model of the non-important and important units of the model is demonstrated in the zoomed image Figure 12. Smaller cell sizes were attempted for all zones, but computational measurements and duration exceeded sufficient run times.

The orientation of a model is often dominated by the flow of groundwater in the target interval, and is often recommended by the reservoir engineer to apply the directional trend as it will have an effect on the behaviour of the CO_2 injection simulation (Yong, 2014). In this project, the measured orientation for groundwater flow in the Foremost Formation is N-S and thus the geostatic model is oriented N-S.

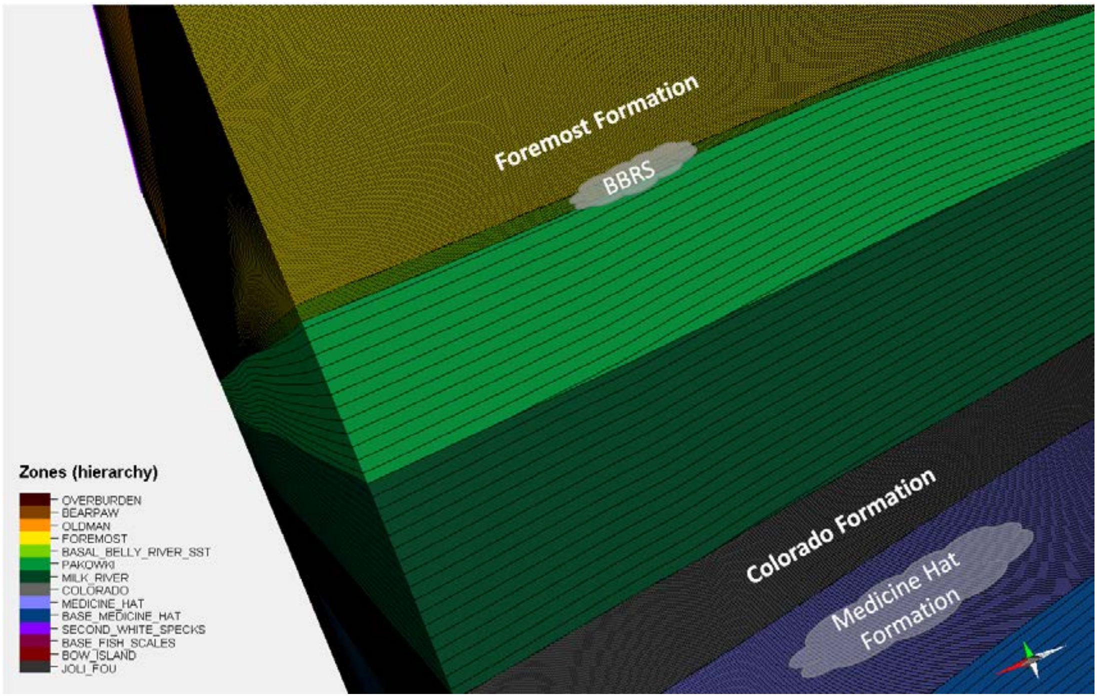

FIG. 12. A zoomed portion of the model to illustrate the blue and green zones that have been layered with cell thicknesses of 5 m. The orange and purple zones above these have been layered with an assigned cell thickness of 0.5 m for the primary injection target and seal intervals.

Well Log Calculations and Property Generation

Effective porosity is the property of interest when relating the permeability and porosity relationship. Within the 198 wells in the project, many included density and neutron porosity logs calibrated to a sandstone density of 2.65 g/cc, and were used to calculate the total porosity utilizing the density-neutron cross-plot calculation seen in Eq – 6 (Zahid, 2007).

$$\phi_{TOT} = \frac{NPSS + DPSS}{2} \qquad \text{(Eq – 6)}$$

The total porosity log has limited significance because it includes the unconnected pore spaces, and does not contribute to the hydraulic behaviour of the rock (Staub et al., 2009). To scale the total porosity to account for the volume of shale, the gamma ray index was computed for the entire 700 m depth using Eq – 7 (Rider and Kennedy, 2011). Based on the area of study, the Late Cretaceous strata are very complicated in that discriminating between sandstones, silty-sandstones, and shales was difficult based on the available gamma ray log data. The clean minimum gamma ray value used was 34 API to represent the sandstones, and the shale maximum value of 175 API was used to represent the shales.

$$V_{SH} \approx I_{GR} = \frac{GR - GR_{(CLEAN)}}{GR_{(SHALE)} - GR_{(CLEAN)}} \qquad \text{(Eq – 7)}$$

For the interest of time, only one value for both the clean and shale gamma ray was utilized to define the shale content with depth. However, for validity of each identified formation, a gamma ray index should be computed to use local maxima and minima values because of the variable origin in organic and radioactive material in each – which can act to skew the data if the index is applied to the entire stratigraphic column but calibrated to a small zone of organic-rich shale.

Under the assumption that the calculated gamma ray index is approximately equal to the volume of shale content in the rock, the effective porosity log was computed using Eq – 8 (Zahid, 2007).

$$\phi_E = \phi_{TOT}(1 - V_{SH}) \qquad \text{(Eq – 8)}$$

As a resultant of only calculating one gamma ray index, this caused for negative effective porosity values in some of the shallow formations. It is known that these Late Cretaceous sediments have not been buried to a great depth, and many of them remain unconsolidated with high pore-water volumes (Pedersen, 2014). The range of effective porosity values required the consideration of limitation, and lead to porosity cut-off values of 0 – 0.35. The upper limit was chosen based on the most frequently observed effective porosity value within the stratigraphic column. Some discretion was applied in using this cut-off due to the presence of coals in the Foremost Formation, as less dense coals can be very porous but can act as impermeable barriers limiting vertical mobility of pore fluids and gases. Coal permeability is often determined by cleats, which are sets of joints that are perpendicular to the top and bottom of the coal seam where two sets of cleats develop an orthogonal pattern (Thomas, 2002). Cleats are natural fractures in coals, and act as conduits for the flow of fluids and gases. Permeability information of the coal zones within the Foremost Formation are not available at present in the public domain (Beaton, 2003), and thus have been assigned a relative permeability of 0 mD.

Permeability

From within the current well log suite there were no permeability logs available, and minimal core data analyses were available for some of the sandstone formations that were modeled. No available core data analyses were conducted on the shale formations in the general area of study. With knowledge of the shaly-sandstones in the Second White Specks Formation, the equation from this unit was applied for the shales in the stratigraphic column. More research is required on the relationship between total and effective porosity, in order to obtain better permeability and porosity relationships using core measurement data.

Permeability was plotted on a logarithmic scale with respect to porosity to obtain the best-fit trend line. The trend line equations were then applied to the effective porosity to generate a permeability property (Table 7).

Table 7. Lists the permeability equations used to calculate the property from effective porosity in each zone. Note that the Overburden, Bearpaw, and Oldman Formation were not modeled due to insufficient shallow data.

Formation Name	Permeability Equation
FOREMOST	PERM_FOREMOST=IF(Zones_hierarchy=3,3920*(PHI_E)-742.8,0)
BASAL_BELLY_RIVER	PERM_BASAL_BELLY_RIVER=IF(Zones_hierarchy=4,3920*(PHI_E)-742.8,0)
PAKOWKI	PERM_PAKOWKI=IF(Zones_hierarchy=5,0.0041*EXP((35.399)*(PHI_E)),0)
MILK_RIVER	PERM_MILK_RIVER=IF(Zones_hierarchy=6,0.0025*EXP((40.649)*(PHI_E)),0)
COLORADO	PERM_COLORADO=IF(Zones_hierarchy=7,0.0041*EXP((35.399)*(PHI_E)),0)
MEDICINE_HAT	PERM_MEDICINE_HAT=IF(Zones_hierarchy=8,7.5149*(PHI_E)-0.3266,0)
BASE_MEDICINE_HAT	PERM_BASE_MEDICINE_HAT=IF(Zones_hierarchy=9,7.5149*(PHI_E)-0.3266,0)
SECOND_WHITE_SPECKS	PERM_SECOND_WHITE_SPECKS=IF(Zones_hierarchy=10,0.0041*EXP((35.399)*(PHI_E)),0)
BASE_FISH_SCALES	PERM_BASE_FISH_SCALES=IF(Zones_hierarchy=11,0.0041*EXP((35.399)*(PHI_E)),0)
BOW_ISLAND	PERM_BOW_ISLAND=IF(Zones_hierarchy=12,0.0185*EXP((38.118)*(PHI_E)),0)
JOLI_FOU	PERM_JOLI_FOU=IF(Zones_hierarchy=13,0.0041*EXP((35.399)*(PHI_E)),0)

Figure 13 and 14 demonstrates the porosity-permeability relationship for the BBRS and Medicine Hat Formation, respectively. Please note that discretion is taken to the permeability relationship with respect to the effective porosity, as this relationship is preliminary and a better identified relationship between effective and total porosity is required in order to utilize a better defined porosity-permeability relationship from core measurements.

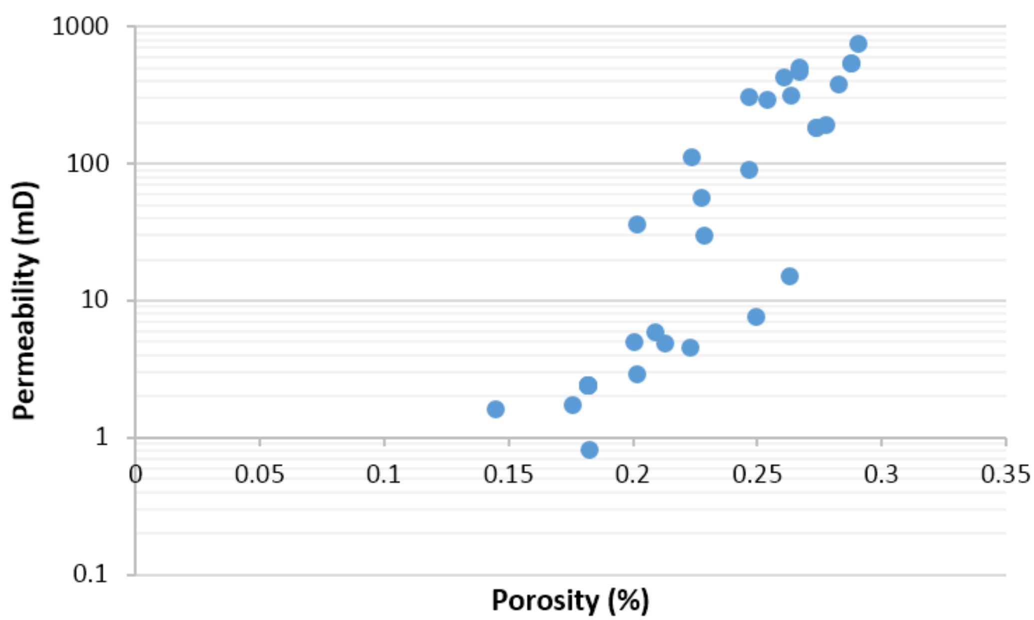

FIG. 13. Porosity and permeability relationship for the BBRS. The data was fit with a linear function that will use the effective porosity to compute the permeability throughout the specified zone. This function was applied to the seal interval, the Foremost Formation, as the BBRS lies within the Foremost Formation.

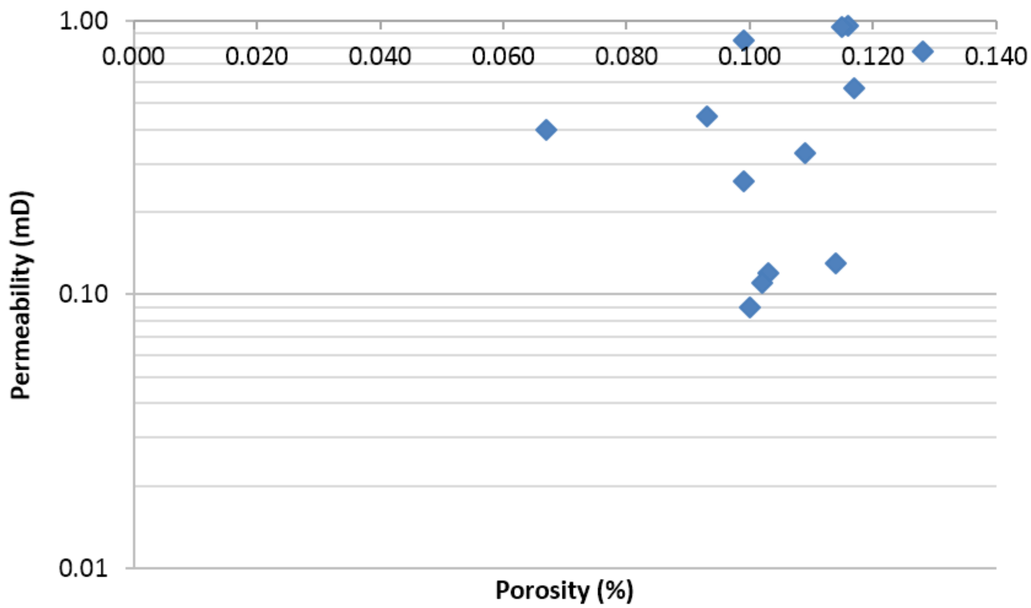

FIG. 14. Porosity and permeability relationship for the Medicine Hat Member. The data was fit with a linear function that will use the effective porosity to compute the permeability throughout the specified zone. This function was applied to the underlying interval known as the Base Medicine Hat.

To achieve the zero relative permeability in the identified coal layers in the Foremost Formation, a facies cut-off (Table 8) using the gamma ray, effective porosity, sonic, and bulk density logs was applied. These were used to obtain a facies log acting to differentiate the coals, shales, silty-sandstones, and sandstones. Once the coals were isolated from the other lithologies, the effective porosities had to be set to equal 0.03. This assumption was made under the knowledge that typically larger ranges of effective porosity lead to greater permeability ranges within a rock. With knowledge that the coal zones have high porosity, the assumed lack of cleating sets the limitation and assumption that the coals are impermeable. Rather than setting the permeability value to zero, a better assumption was to attribute the coals to having very low permeability (Butch, 2014).

Table 8. Cut-offs used on well log data to isolate the coals in the Foremost Formation from the shales, silty-sands, and sandstones in the model.

Facies	Log Cut-off
Coal	RHOB<2; DT>130; PHI_E>0.26; PHIE_E=0.03
Shale	GR>95
Silty-Sand	50<GR<95
Sand	GR<50

*Note: RHOB=Bulk Density; DT= P-Sonic; PHI_E= Effective Porosity; GR= Gamma Ray

Upscaling Well Logs and Property Generation

From the assigned cell thickness and defined layering of each zone, the well logs were then upscaled into a cell property. Upscaling the well log acts to average the range of values of the specific log within the range of the assigned cell thickness. In this case for the target and seal intervals, the values for effective porosity were averaged over 0.5 m. In the units of low importance, the values for effective porosity were averaged over 5 m. Once the effective porosity log was transformed into a cell property, data analysis and 3-D model population was completed for each zone.

Petrophysical Modeling

Data Analysis of Properties

Data analysis was completed for the constructed surfaces, horizons, and petrophysical modeling of the two geological properties using the outer 10 km radius to produce variogram statistics from the 198 wells. The spatial variance and continuity between two wells and more is dependent on not only the distribution of the petrophysical attribute, which is the porosity and permeability relationship (Statios, 2004), but also the distribution of the wells themselves.

Due to the small area (1 km^2) of the GFRS site, continuity of properties in the geological region was assumed. This was completed by defining an appropriate regression curve and values to the nugget, sill, and range of the data in all three vertical, major, and minor directions. The definitions of the settings are listed below in Table 9.

Table 9. Variogram settings and the definitions as to how data was analyzed as described by Statios (2004) and Barnes (2014).

Variogram Setting	Definition (Statios; Barnes 2014*)
Regression Curve	Best-fit curve to input data (includes linear, exponential, spherical models)*.
Sill	The variance; typically given a value of 1.0 if the data has a normal distribution.
Range	The distance at which the variogram reaches the assigned sill.
Nugget Effect	The sum of the error within data acquisition and geological microstructure. Error within the data as a function of instrument calibration or location assigned to the measurement increases the nugget effect. Little/sparse data often leads to a higher nugget effect too.

The variogram settings were applied within the 5 km^2 model to honour the surrounding geological and structural trends of the input data. The variogram analysis for the BBRS and Medicine Hat Member are displayed in Figures 15 and 16.

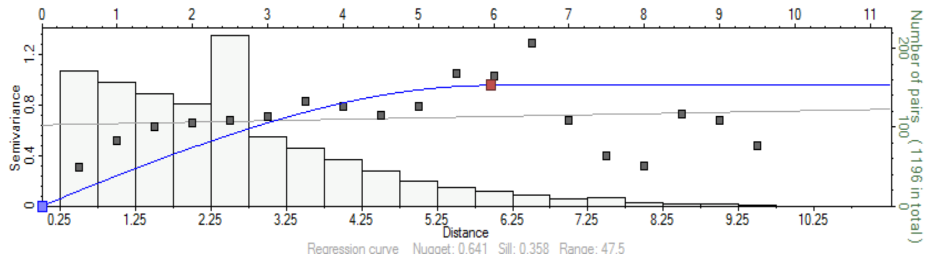

FIG. 15. The experimental variogram and the settings chosen to display the variability of the effective porosity in the BBRS primary target interval.

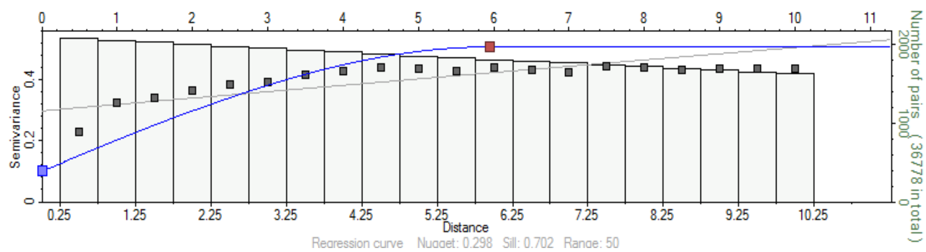

FIG. 16. The experimental variogram and the settings chosen to display the variability of the effective porosity in the Medicine Hat secondary target interval.

Gaussian Random Function Simulation Algorithm

The model was populated with the effective porosity and permeability property values by utilizing the Gaussian Random Function Simulation algorithm in Petrel™ 2014.1. It is considered to be a conditional simulation algorithm that incorporates both kriging and unconditional simulation (Schlumberger, 2014). Under the assumption that the data have a normal distribution, the Gaussian Geostatistical Simulation (GGS) algorithm is more advantageous than kriging. The algorithm is stationary in that over the spatial domain of the input data, the values for the mean, variance, and spatial structure do not change. Kriging produces a smoothed output because it is based on a local average, whereas the GGS inserts the local variability in the data that is lost. The conditional simulation portion of the algorithm then honours the input data and is able to model the expected variability in property distributions (Schlumberger, 2014). The unconditional simulation portion of the algorithm does not replicate the data's mean, variance, or semi-variogram, and thus does not honour the input data. The difference between the two simulations is where the modeled data is placed on the cell grid. Variation in the sample location might occur because the modeled values are placed at the grid cell center and thus might not be in the exact location of the input sampled data point. Whereas in the unconditional simulation, a prediction map of the modeled property may display areas of high and low effective porosity values, but not in the location of where they exist in the input data. (Esri, 2012)

The algorithm is parallelized, allowing for fast computation time for multiple model iterations. As well, Petrel™ offers a co-kriging option within the algorithm function itself. This option can be used if there is a known geological feature with specified properties, and can be co-krigged into the simulation to honour that data. (Schlumberger, 2014)

Excluding the Overburden, Bearpaw, and Oldman Formation, the GFRS model was populated for both permeability and porosity to a depth of 700 m (to the top of the Mannville Group). The fully populated effective porosity model is shown in Figure 17.

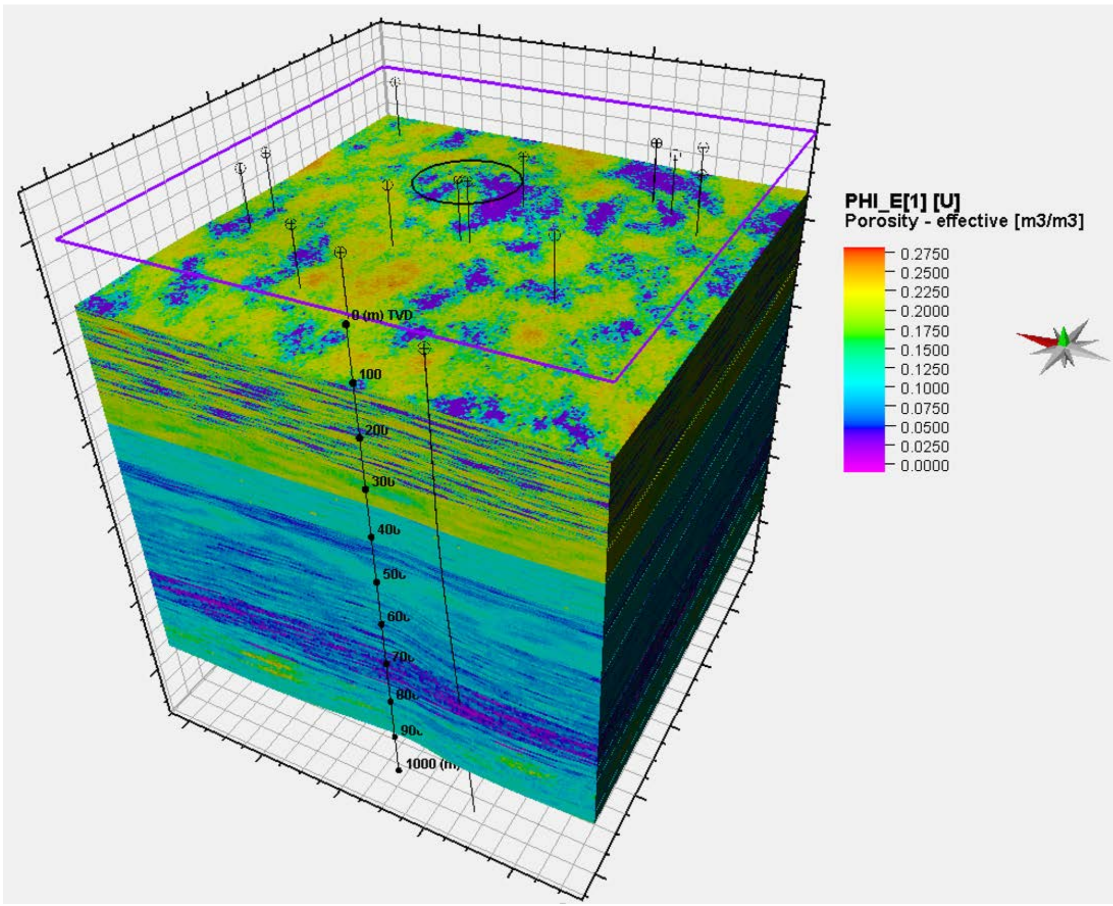

FIG. 17. The 5 km x 5 km property model of the GFRS with each zone populated with effective porosity. The highest effective porosity modeled is 27.5% (red) and lowest is 0% (pink).

In Table 10, the statistical range of effective porosity and permeability values are listed for the target and seal intervals. An earlier version of the 5 km^2 property model was computed in May 2014, with different porosity-permeability equations used to populate the model. The change between the modeled effective porosity ranges for the seal and target intervals is small. However, the opposite is true when comparing the permeability ranges for the primary seal and target intervals. It has been considered that the interpretation of the larger 300-360 mD values represent the air permeability at the surface, and would need to be corrected for overburden pressure, water saturation of the rock, as well for the fluid being injected (Pedersen, 2014). The lower 55-85 mD permeability values are most likely closer to the permeability values that the injected CO_2 would see in the subsurface with corrections applied (Pedersen, 2014). Also note, the permeability equations used for the primary and secondary injection intervals to obtain these two properties was taken from the Milk River Formation within the stratigraphic column. The depositional environment and nature of the sediments in this interval are much different than those of the BBRS, which may have artificially dampened the property ranges.

Table 10. Range of effective porosity and permeability values for the primary and secondary target and seal intervals computed in May and November 2014.

Interval	Type	Effective Porosity (%)		Permeability (mD)	
		May 2014	Nov 2014	May 2014	Nov 2014
Foremost Formation	Seal	0-26	0-28	0-55	0-360
BBRS	Primary Target	0-25	0-27	0-85	0-300
Colorado	Seal	0-17	0-14	0-0.46	0-0.57
Medicine Hat Member	Secondary Target	0-13	0-18	0.02-2.5	0-1

P10/50/90 Framework

As described by Mao-Jones (2012), “uncertainty should be modeled with probability distributions (a range of possibilities combined with probabilities assigned to each of those possibilities).” In order to communicate the uncertainty that is within the property model, the P10/50/90 framework was used. It refers to the data that ranges between the 10^{th}, 50^{th}, and 90^{th} percentiles. The P10 is typically referred to as the conservative outlook or the “lowest value that the expert thinks that the uncertain variable could be” (Mao-Jones, 2012). The P50 is typically referred to as the typical or “most likely value” (Mao-Jones, 2012). Lastly, the P90 is often referred to as the most optimistic, or the “highest values that the expert thinks the variable could be” (Mao-Jones, 2012). Any data points that lie before the P10 and after the P90 are very unlikely scenarios (Zaluski, 2014).

This framework was used to model the effective porosity and permeability properties clipping to a 1 km^2 filter about the main 7-22 well in the GFRS study area. A workflow was constructed to model the effective porosity for 40 iterations. Due to the capacity of computation power, there was a limitation on the number of iterations that could have been run. Any more than 40 iterations of property modeling crashed the project. It is understood that the greater number of model iterations will produce a data distribution closer to a normal score. Once the pore volumes were modeled, a total of 40 bins and 19 bins were used to organize the data by frequency and range and plotted to view the distribution for the primary (Figure 18) and secondary (Figure 19) target interval, respectively.

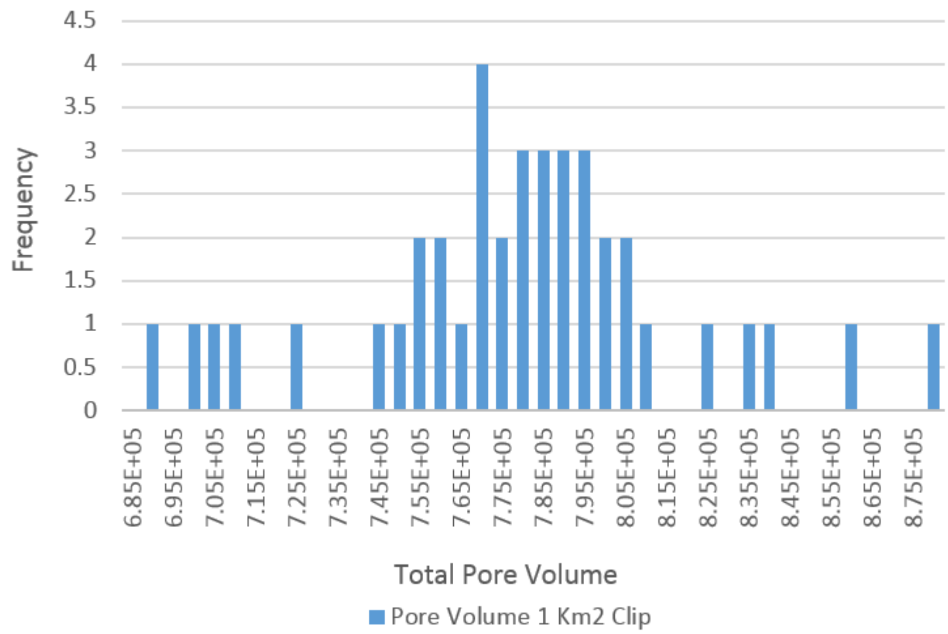

FIG. 18. Assigned pore volume bins based on pore volume sum data, plotted with occurrence frequency for the BBRS in a 1 km^2 filter about the 7-22 well.

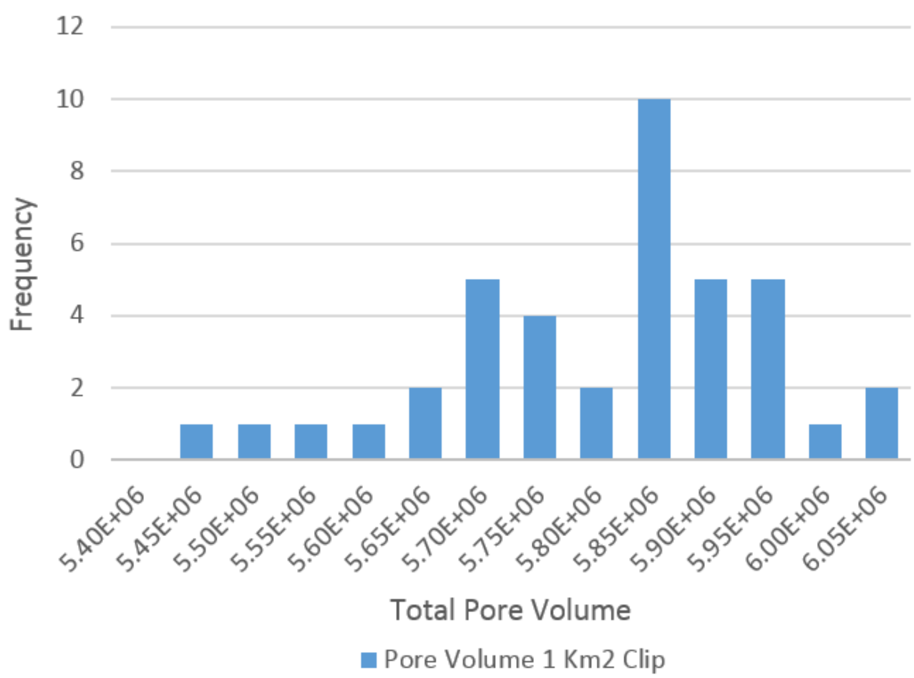

FIG. 19. Assigned pore volume bins based on pore volume sum data, plotted with occurrence frequency for the Medicine Hat Member in a 1 km^2 filter about the 7-22 well.

For each P10/50/90 percentile, there is an attributed pore volume to each and these three values for each target interval will be given to the reservoir engineer to be utilized in the simulation for the CO_2 injection. In Figures 20 and 21, the P10/50/90 percentiles are labeled on the graph identifying the ranges of data for the effective porosity in the BBRS and the Medicine Hat Member, respectively.

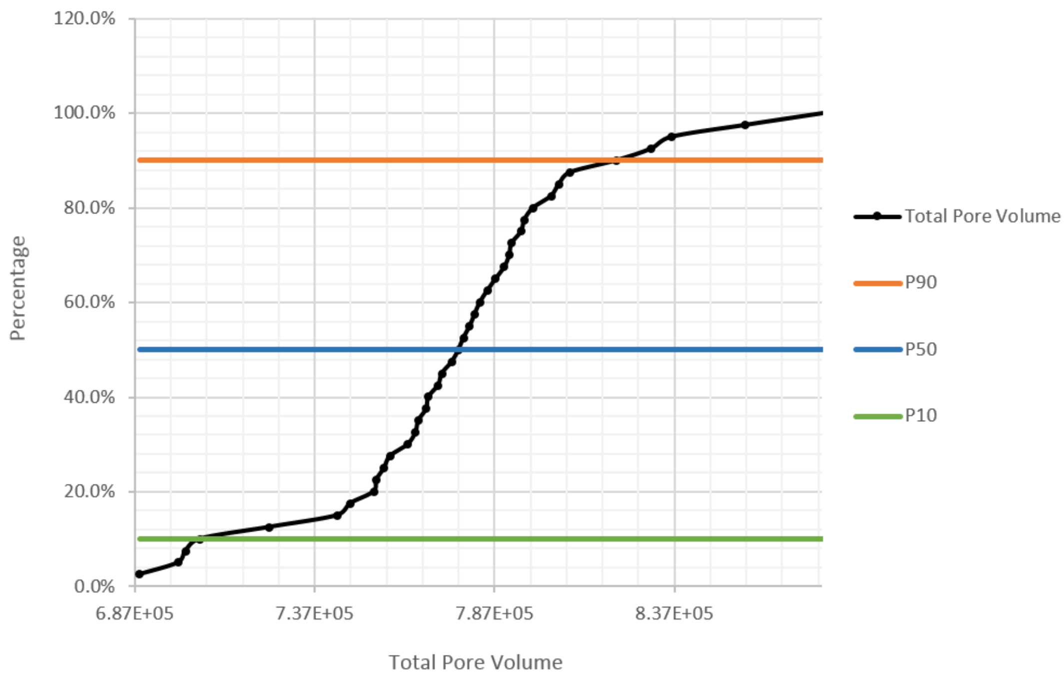

FIG. 20. Total pore volume data for the BBRS in the 1 km^2 clipped region with the identified P10/50/90 percentiles for uncertainty.

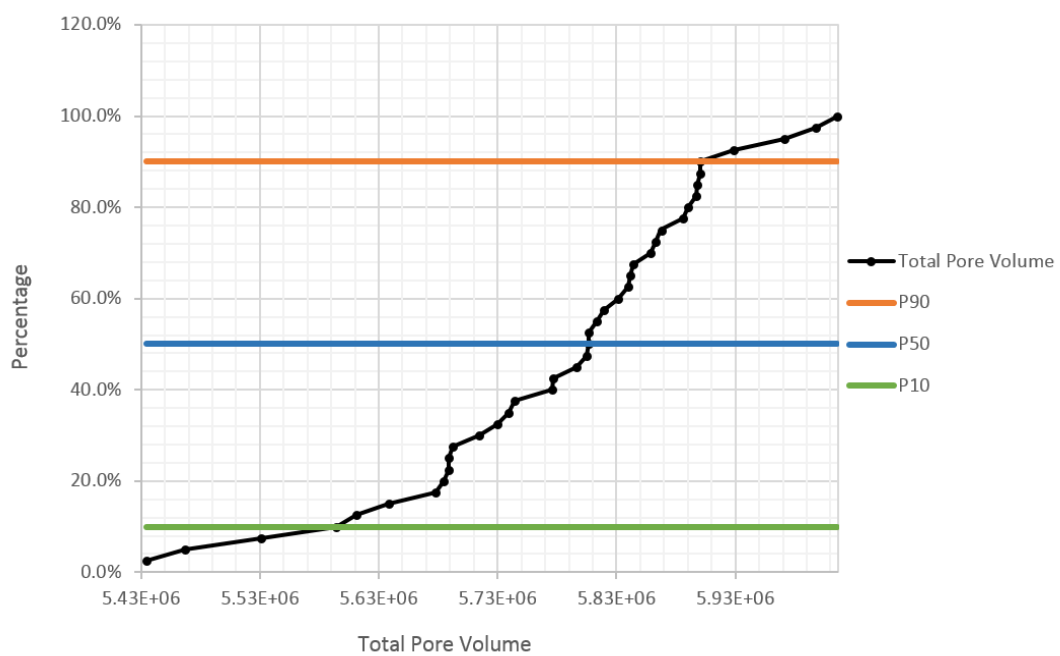

FIG. 21. Total pore volume data modeled for the Medicine Hat Member in the 1 km^2 clipped region with the identified P10/50/90 percentiles for uncertainty.

Porosity Thickness Maps

Effective porosity net thickness maps were created for the BBRS and the Medicine Hat Member. Using Eq – 9 (Schlumberger, 2014); the two properties modeled spatially in 3-D are multiplied by the formation zone thickness to obtain a 2-D map view of each reservoir.

$$z = sum[P(i) * Height(i)] \qquad \text{(Eq – 9)}$$

The *P(i)* in Eq – 9 represents the property that will be mapped. In this case, the effective porosity and permeability at all positions (x,y) on each given surface was used and produces a smoothed result. The effective porosity thickness maps of the BBRS for the "typical" P50 from the P10/50/90 framework are displayed in Figures 22 and 23, respectively.

The produced effective porosity net thickness maps serve as a perspective of how the property are distributed with depth, and can be used to construct further investigation planning such as potential drilling areas or new areas that require greater 3-D seismic coverage. Permeability thickness maps will be constructed in part of the next steps of the GFRS project.

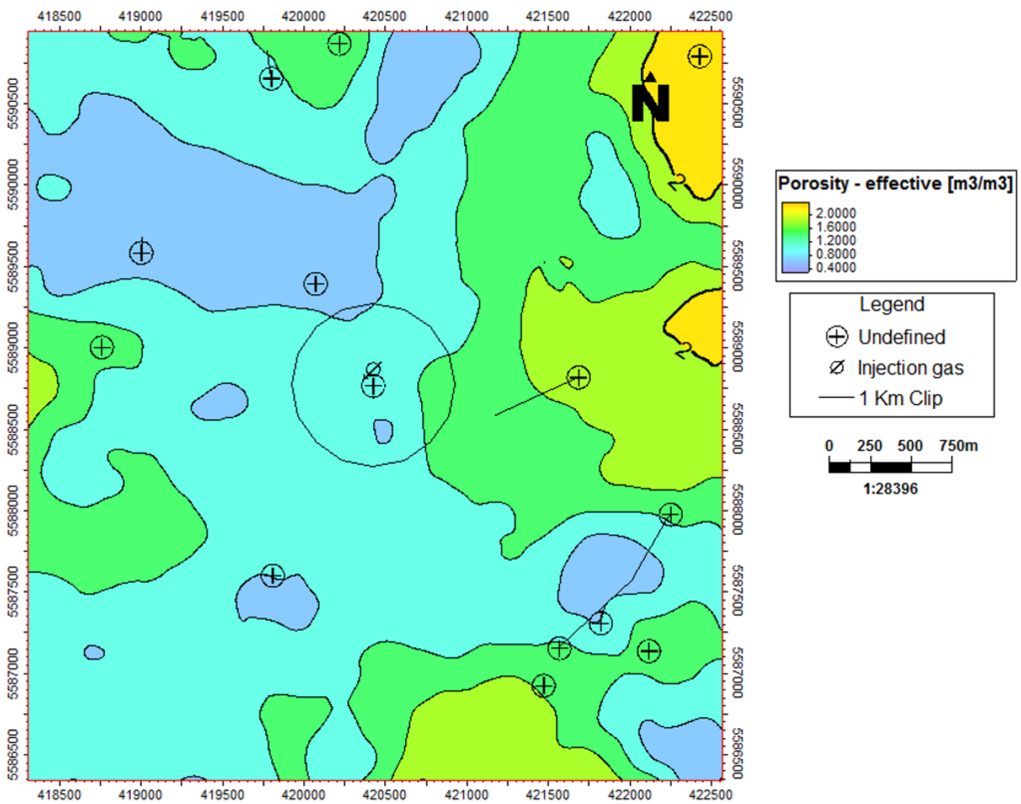

FIG. 22. The "typical" P50 pore volume realization thickness map for the BBRS in the GFRS area. Pore volume realization iterations were clipped to 1 km^2 about 7-22.

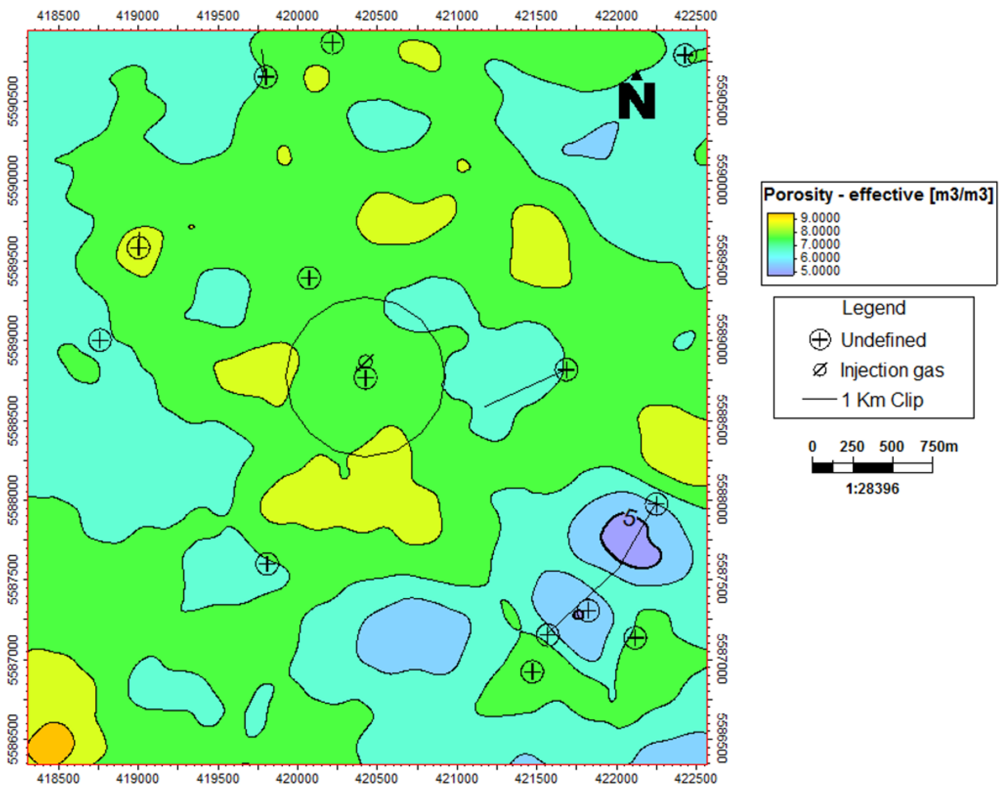

FIG. 23. The "typical" P50 pore volume realization thickness map for the Medicine Hat Member in the GFRS area. Pore volume realization iterations were clipped to 1 km^2 about 7-22.

4 KM X 5 KM GEOSTATIC GEOPHYSICAL MODEL

With a previously constructed 5 km by 5 km property model of the GFRS study area of which includes only geological and statistical data, a 4 km x 5 km geophysical model was constructed. It entails well-ties that were used to determine the time-depth relationship (TDR) with respect to the two 3-D seismic reflection volumes in the project. Velocity modeling enabled the seismic data and respective horizon interpretations to be converted to depth, which were used to update the surfaces in the 5 km^2 property model. The property and geophysical model will be clipped to a 1 km^2 area, resulting in an integrated geostatic model about the main 7-22 well. This will be used for the CO_2 fluid injection simulation, given the P10/50/90 statistics for the effective porosity and permeability properties.

Horizon Tracking

The interpretation of subsurface horizons was completed after a thorough understanding of the impedance change at each reflector. The changes in acoustic impedance will affect whether the reflector is a trough or a peak. It is also important to remain constant in identifying these in the seismic section, thus the seismic processor may or may not have changed the polarity of the data. In this data set, the North Sea convention was used, where a peak can be identified as going from low to higher acoustic impedance and a trough as going from high to lower acoustic impedance values.

For the 3-D vintage and newer seismic volumes, manual and seeded 3-D auto-tracking were used. The seeded 3-D auto-tracking option enables an algorithm to deploy the picked trace based on a recognition pattern and a seed confidence level. These can be determined as peaks, troughs, zero crossing, or none (flat). The seed confidence level determines the acceptance or rejection of a horizon expansion based on the confidence percentage assigned to the tracker to apply to the seed values (Schlumberger, 2014). Depending on the lateral continuity and strength of the subsurface reflectors, manual interpretation was used in order to capture the reflector through dipping and weak amplitude regions of the section. Both the amplitude and proximity was given the priority during interpretation.

The two seismic volumes did not perfectly align with each other in time. This is a post-processing result of different seismic reflection data acquired at different times. It was assumed that the newest 3-D/3-C dataset acquired in May was hung appropriately at 800 m. This required a bulk shift of -32 ms, which was visually determined and applied to the 3-D/1-C seismic data.

For two of the subsurface horizons at greater depths below the target injection intervals, it appeared that the newer seismic data set, even after the 1997 data was bulk shifted still had a difference in where the reflector was in time. These include the Second White Specks Formation and the Mannville Group. This resulted in conflicting interpretation of where the subsurface reflector was located at depth, not only giving edge effects but also placing the horizon at a greater time than what was interpreted on the 1997 3-D volume. A possible reason behind the difference in reflector location could be a difference in the phase of the data, as the 1997 3-D volume was recorded using a dynamite source and the May 2014 3-D volume was recorded using a vibroseis source. As well, for each 3-D seismic reflection volume lies different amount of acquisition noise, as well as different processing steps and techniques that may have been used which can result in phase differences.

Well-Tie Process

In the Petrel™ software, there are two steps in completing a well-tie. First is the sonic calibration, which corrects for any drift in measurement with depth. The second step involved the actual synthetic generation process, where the TDR is applied to the sonic log in the well. To develop the TDR with respect to previously interpreted formation tops from well logs, either a sonic log or check-shot surveys can be used (Abbas, 2009). In this project, no check-shot data was available and so the TDR was developed by using the calibrated sonic log in each well. The wells that were chosen to be used in the well-tie process are those with sonic and bulk density log curves, which are required to compute the acoustic impedance and reflectivity.

The wavelet used to create the synthetic seismograms for the seismic well-tie process was an Ormsby zero-phase wavelet (10/50-75/95 Hz), with a sampling interval of 2 ms and is 200 ms in length (Figure 24).

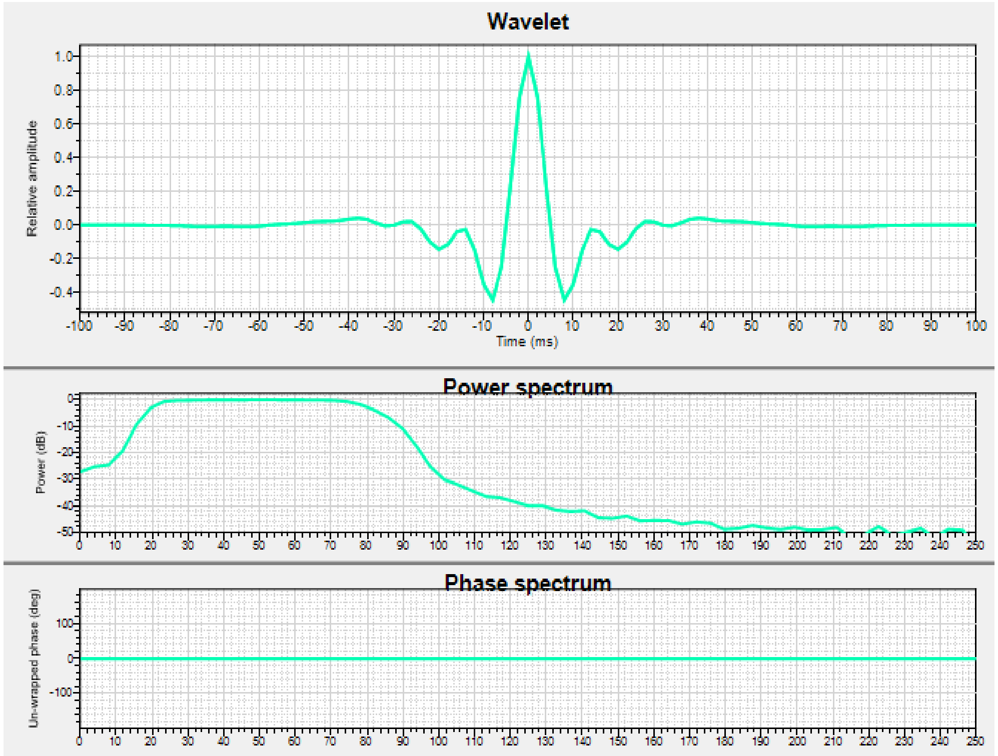

FIG. 24. The Ormsby wavelet (10/50-75/95) wavelet and its phase spectrum that is used in the convolution with the reflection coefficients to obtain the synthetic seismograms for each of the eight wells used for the well-tie process.

A synthetic interpretation step is required, as the wavelet applied is not time-variant and there is no noise contribution factored into the simple convolution matrix. The differences between the synthetic data and recorded seismic data are a result of this procedure. For example the strength of reflectors may differ, and the reflector may appear delayed in time by a few ms. Minor stretch-squeeze adjustments were applied to align major subsurface reflectors in the synthetic with those of the seismic (Figure 25). Assigned time shifts through stretch-squeeze adjustments often are given a negative connotation, as it can be seen as artificially fitting the data to allow the TDR to match. The well tops of the different subsurface formations can be seen tied to the horizon interpretation on the seismic section in time in Figure 26. It is important to QC the adjustments applied to the synthetic seismogram. This can be done through extracting the wavelet from the synthetic after the applied time-shifts to see how closely the extracted and applied Ormsby wavelet match. The extracted wavelets from each well that was tied to the two seismic volumes can be seen in Figure 27 (A-H).

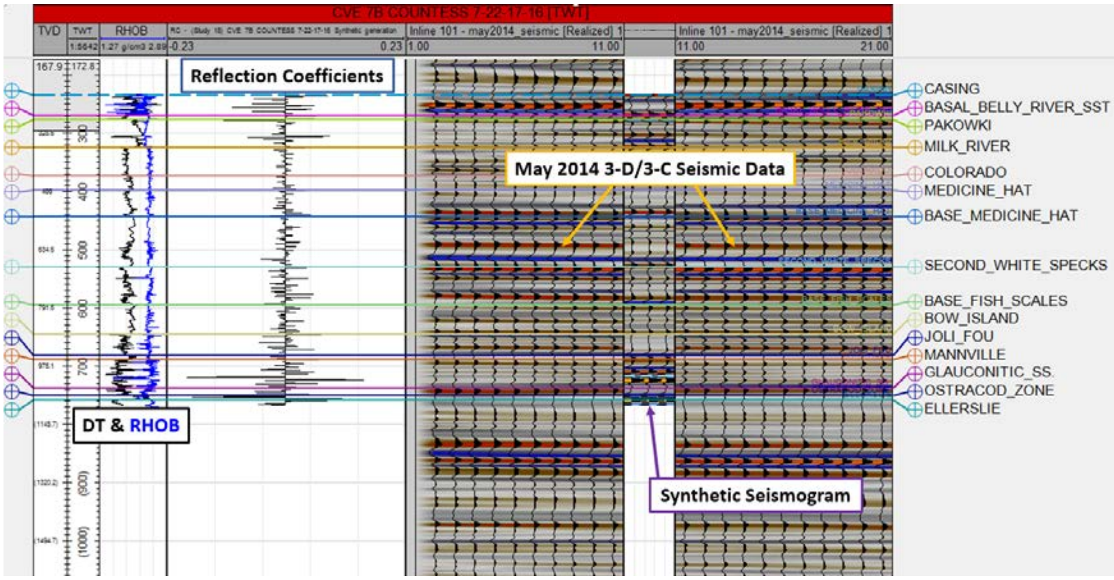

FIG. 25. The well section window in Petrel™ 2014.1, where the well-tie process was completed. Subsurface formation well tops that have been tied in time (ms) are listed.

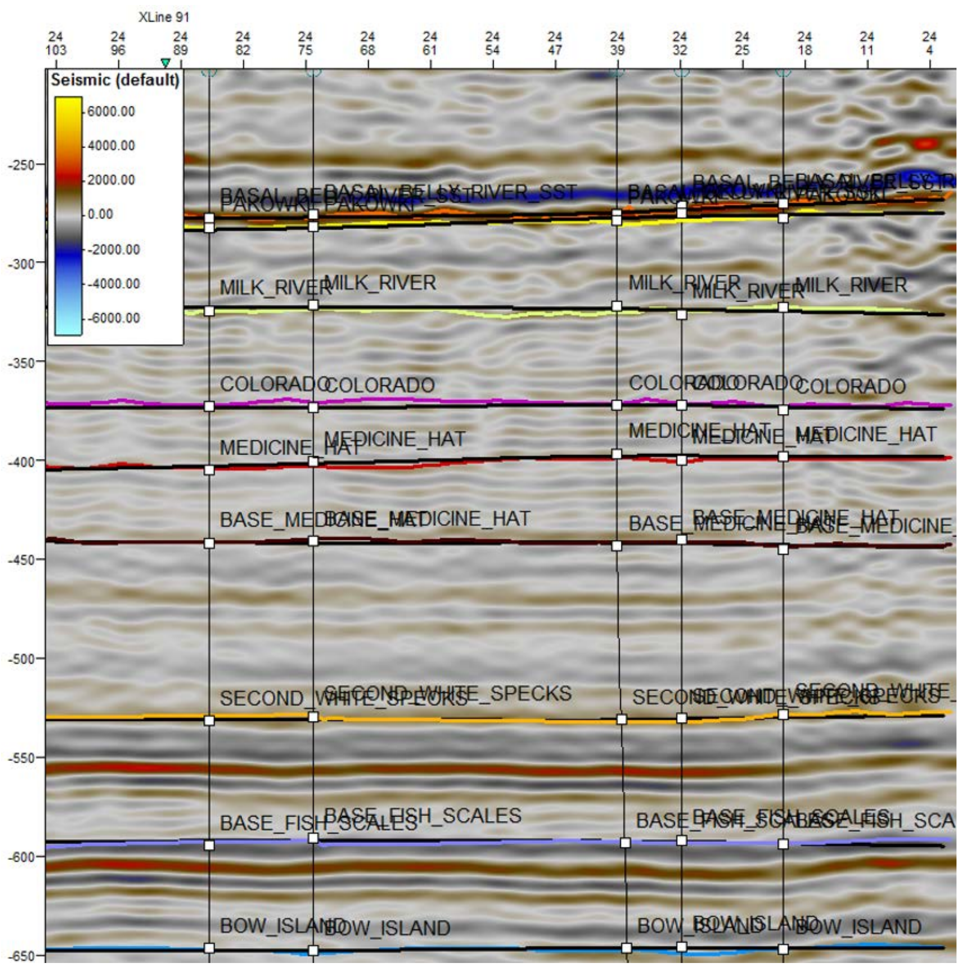

FIG. 26. Displays the 1997 3-D/1-C vintage seismic section with five wells that have been tied in time to the seismic horizon interpretation as a result of the well-tie process.

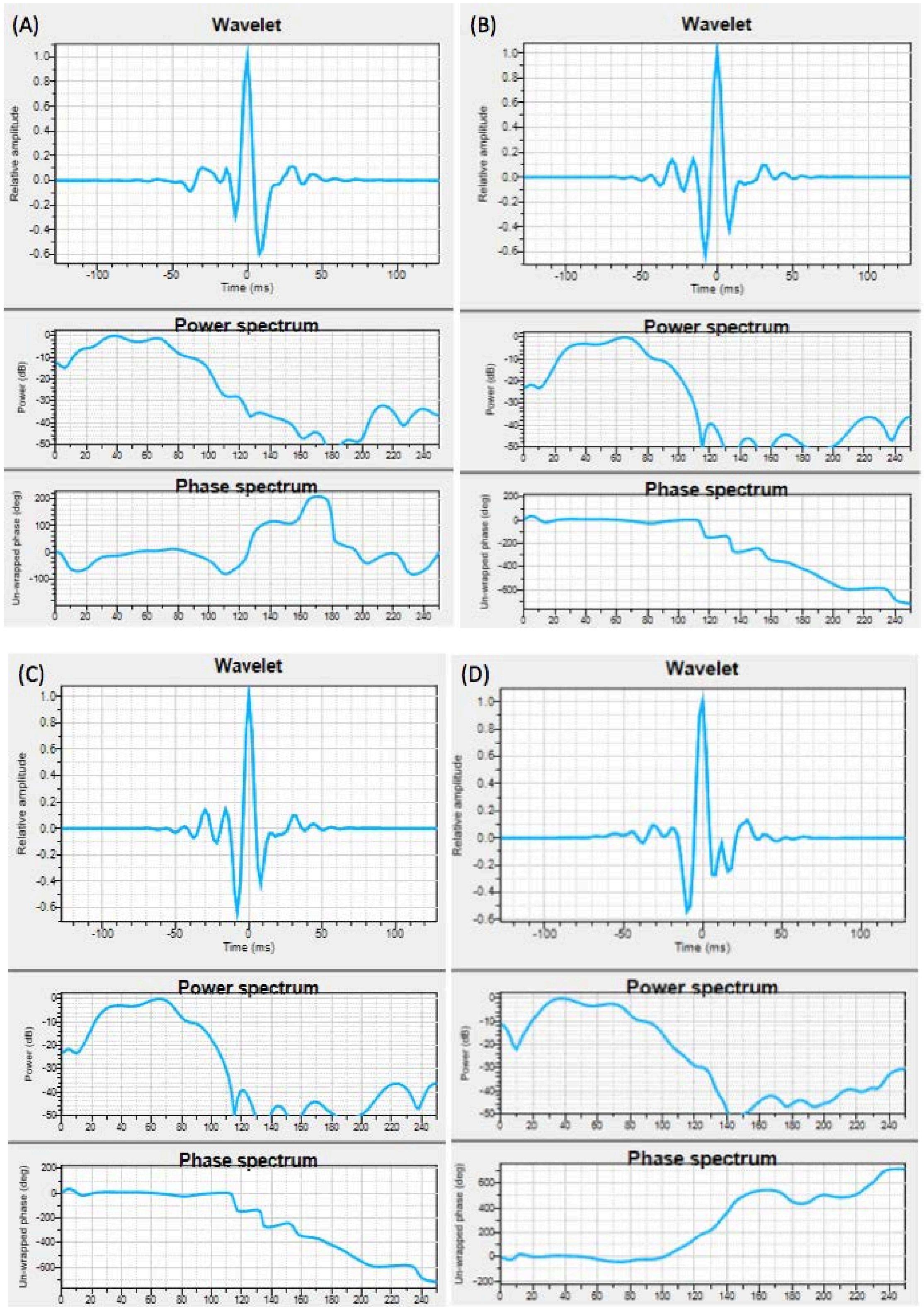
(A)
Wavelet
Relative amplitude
Time (ms)
Power spectrum
Power (dB)
Phase spectrum
Un-wrapped phase (deg)
(B)
Wavelet
Relative amplitude
Time (ms)
Power spectrum
Power (dB)
Phase spectrum
Un-wrapped phase (deg)
(C)
Wavelet
Relative amplitude
Time (ms)
Power spectrum
Power (dB)
Phase spectrum
Un-wrapped phase (deg)
(D)
Wavelet
Relative amplitude
Time (ms)
Power spectrum
Power (dB)
Phase spectrum
Un-wrapped phase (deg)

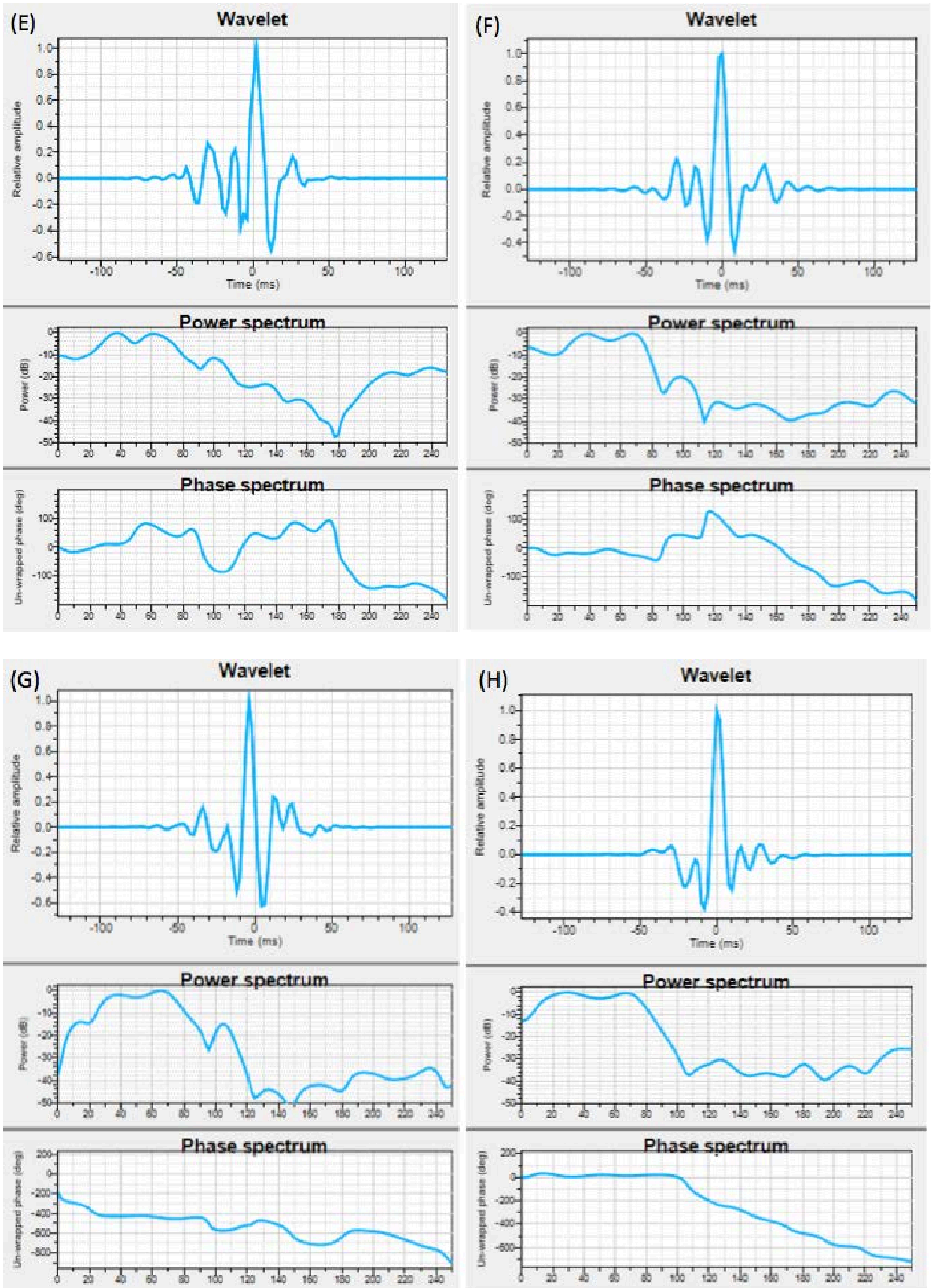

FIG. 27. Extracted wavelets, respective amplitude power, and phase spectrum from each well tied to the 2014 and 1997 3-D seismic volume. Each wavelet has a window length of 440 ms. (A) Extracted from 11-22-17-16W4 tied to 1997 3-D. (B) Extracted from 14-28-17-16W4 tied to 1997 3-D. (C) Extracted from 15-21-17-16W4 tied to 1997 3-D. (D) Extracted from 7-21-17-16W4 tied to 1997 3-D. (E) Extracted from 9-26-17-16W4 tied to 1997 3-D. (F) Extracted from 6-23-17-16W4 tied to 1997 3-D. (G) Extracted from 11-27-17-16W4 tied to 1997 3-D. (H) Extracted from 7-22-17-16W4 tied to 2014 3-D.

Contoured Surface Generation in Time

As a result of the horizon tracking, a grid is attached to the interpreted horizons in 3-D. Surfaces for the specific formations to be represented in the seismic section must be produced in time (ms). By using the Make/Edit Surface process, the interpreted horizon grid can be used to create the surface. In order to convert the seismic sections to depth, a velocity model with subsurface horizons in time is required.

The time surfaces were constructed using input from both the TDR from the synthetic seismogram and well-tie process, as well as the independent horizon interpretation that was completed on the 3-D seismic volumes. The well tops in time were weighted at 75% and the seismic interpretation in time was weighted at 25%. The seismic interpretation of subsurface reflectors can be considered to be ambiguous to the interpreter, which is the reason behind weighting the interpretation less than the well-tie - especially where amplitudes are small and a clear horizon is difficult to depict. The surfaces can be seen in Figures 28-31.

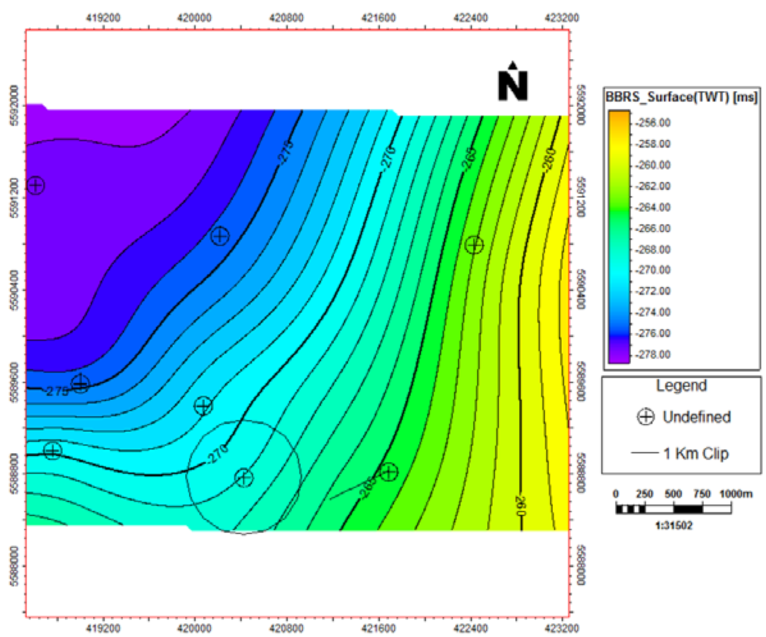

FIG. 28. The BBRS (primary injection interval) surface as a result of seismic horizon interpretation on both 1997 and 2014 3-D volumes in time. The eight wells displayed are those of which have well-ties to the seismic volumes.

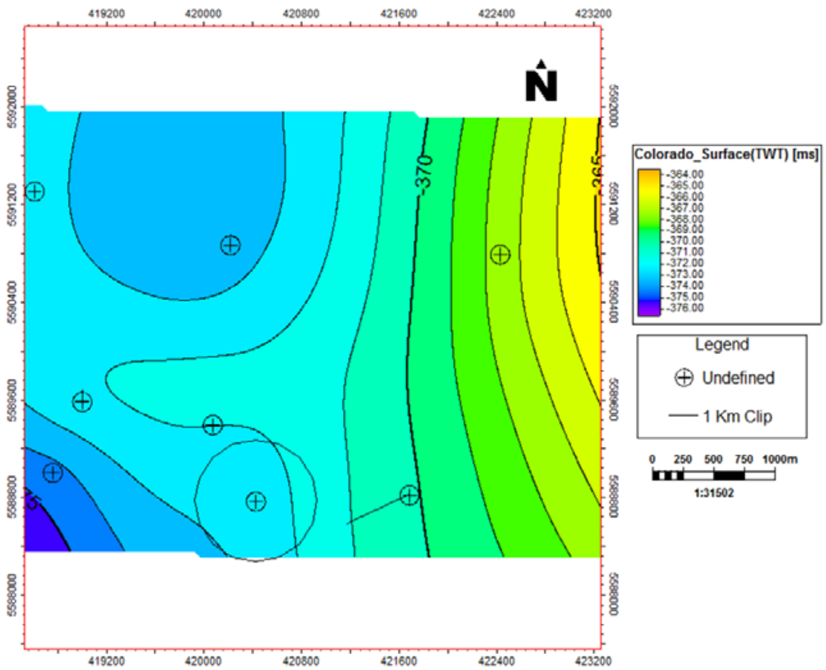

FIG. 29. The Colorado Formation (secondary seal interval) surface as a result of seismic horizon interpretation on both 1997 and 2014 3-D volumes in time. The eight wells displayed are those of which have well-ties to the seismic volumes.

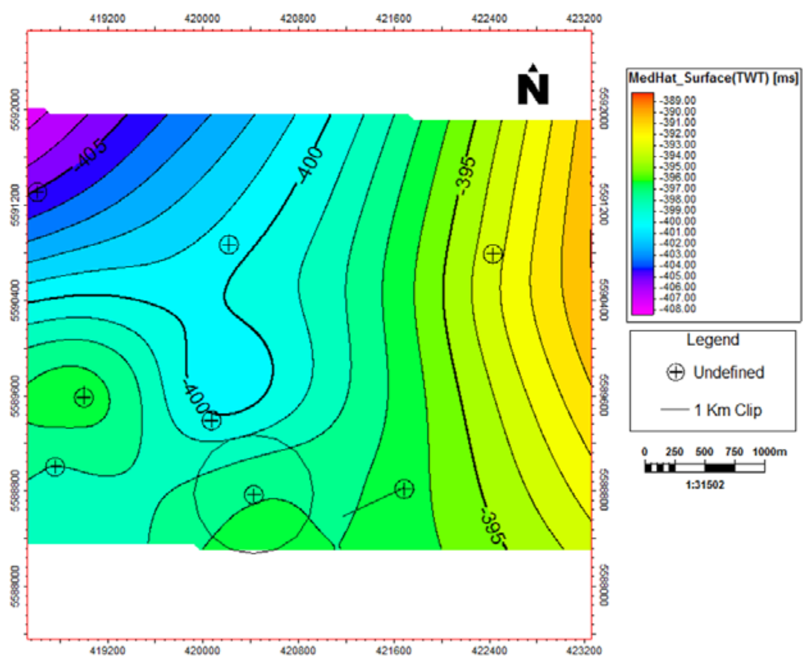

FIG. 30. The Medicine Hat Member (secondary injection interval) surface as a result of seismic horizon interpretation on both 1997 and 2014 3-D volumes in time. The eight wells displayed are those of which have well-ties to the seismic volumes.

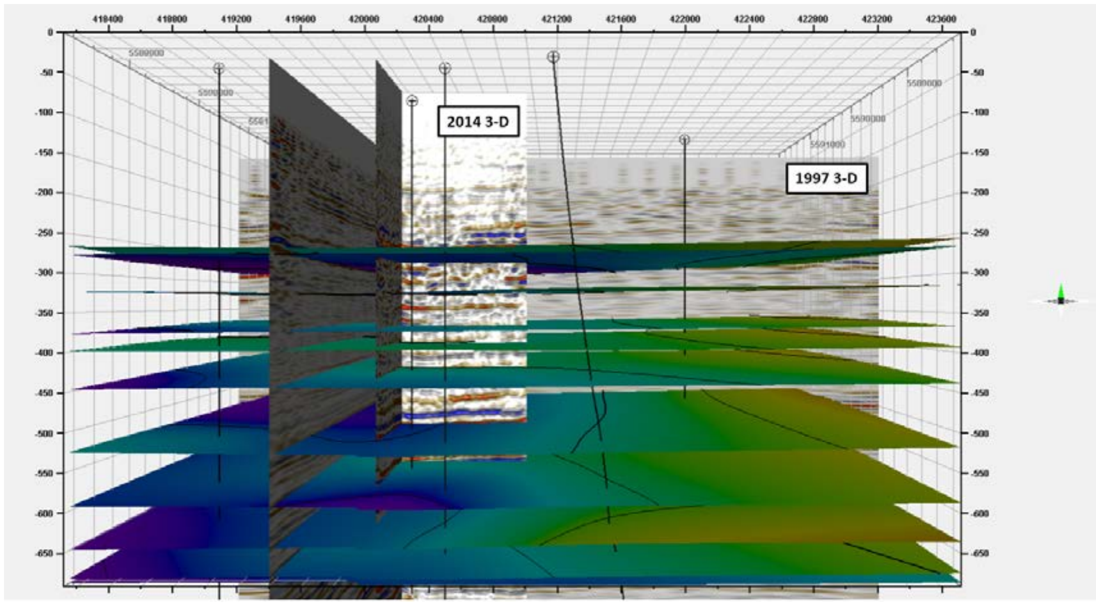

FIG. 31. A display of the two 3-D seismic reflection volumes, 8 wells with completed well-ties, and time surfaces intersecting these as a result of seismic horizon interpretation.

Isochron Maps of Target and Seal Intervals

Isochron maps were generated for the Foremost Formation, BBRS, Colorado Formation, and the Medicine Hat Member. The contoured map displays the variation in time between two seismic reflectors in the subsurface. The isochron maps for the target and seal intervals can be seen in Figures 32-34.

The process of creating a thickness map is the same and utilizes the isopoints equation (Eq – 1) of two subtracting surfaces, where the only the mode (depth/time) differentiates the type of map produced. Due to the lack of complex structure in the GFRS study area, in theory, the correlated isopach and isochron maps should be the same if constant velocity is present. Note that there is no contoured isochron map for the Foremost Formation seal interval, as this horizon was not interpreted on the 3-D seismic volumes and was not a well top used during the well-tie process.

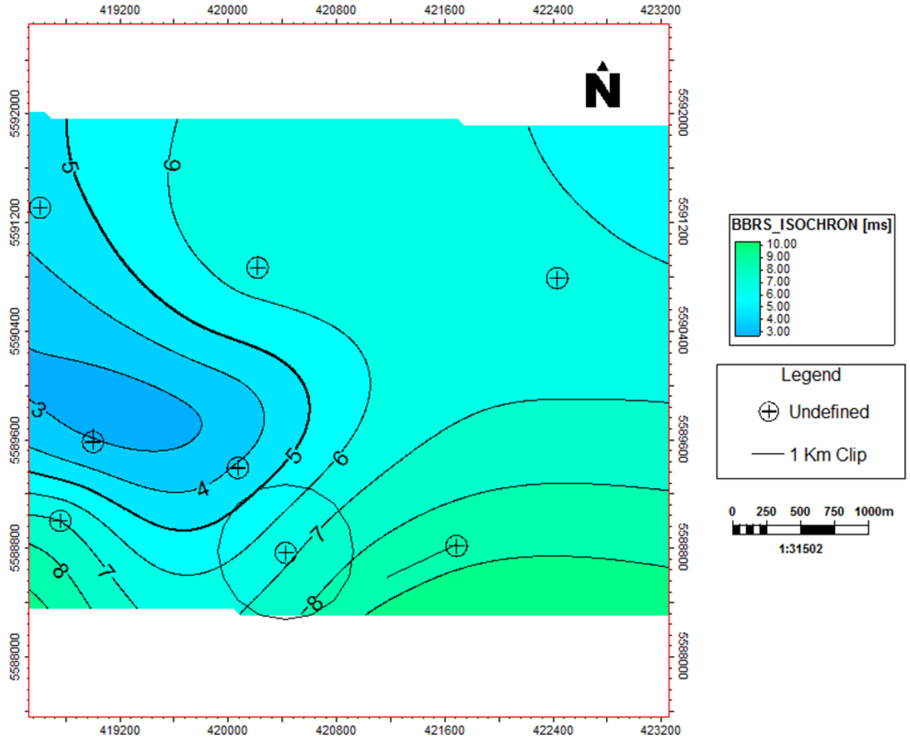

FIG. 32. Contoured isochron map in time for the BBRS injection interval. The eight wells displayed are those of which have well-ties to the seismic volumes.

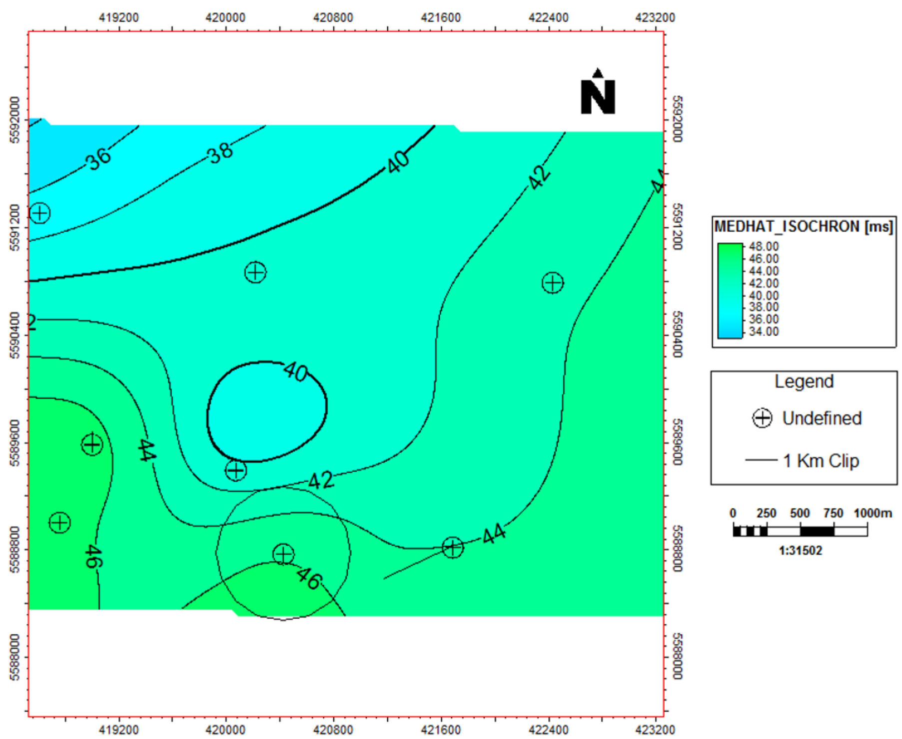

FIG. 33. Contoured isochron map in time for the Medicine Hat Member injection interval. The eight wells displayed are those of which have well-ties to the seismic volumes.

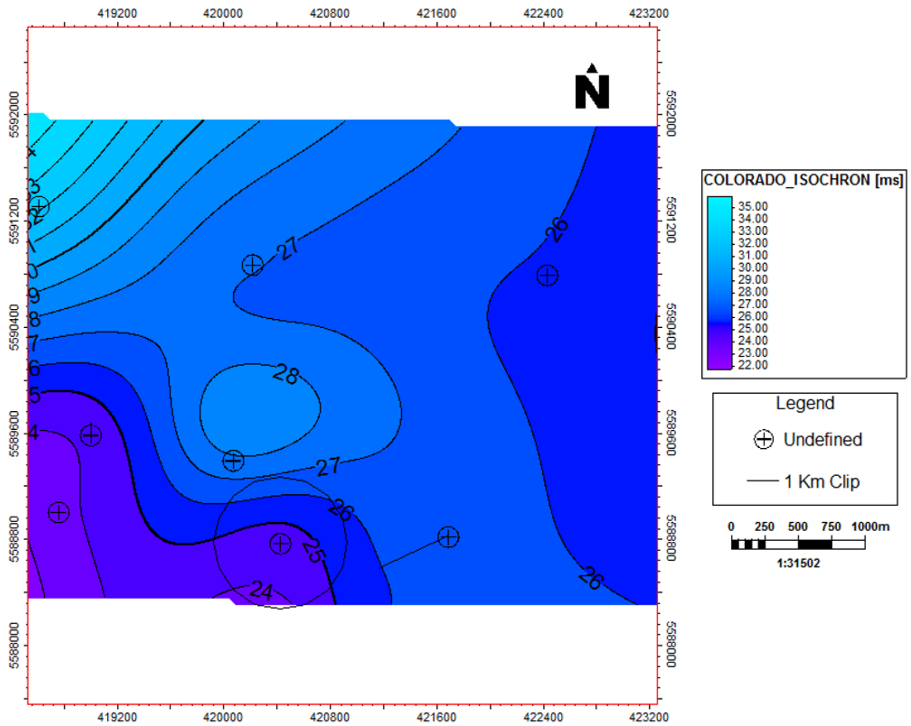

FIG. 34. Contoured isochron map in time for the Colorado Formation seal interval. The eight wells displayed are those of which have well-ties to the seismic volumes.

Depth Conversion

The 4 km x 5 km geophysical model which includes well tops interpreted in time as a result of the 8 well-ties, and the two seismic horizon interpretations for the two 3-D seismic volumes must be domain converted to depth in order to integrate the two geostatic models. The depth conversion was completed by using a Velocity Modeling process in Petrel™. This process utilizes the TDR obtained from the well-ties competed in the project. Velocities of the subsurface intervals may however be erroneously derived if there were many stretch-squeeze adjustments applied to the synthetic seismogram. A velocity constant (V0) is required at each time surface, and this was obtained from the TDR from computing the 8 well-ties (Figure 35).

Base		Correction				Model
Surface	BBRS_Surface(TW	Well tops	BASAL_BELLY_RIVER_SST (Well tops)	V=V0=Vint	V0: Constant	2213.7
Surface	Pakowki_Surface(T	Well tops	PAKOWKI (Well tops)	V=V0=Vint	V0: Constant	2195.3
Surface	MilkRiver_Surface(T	Well tops	MILK_RIVER (Well tops)	V=V0=Vint	V0: Constant	2628.6
Surface	Colorado_Surface(T	Well tops	COLORADO (Well tops)	V=V0=Vint	V0: Constant	3252.17
Surface	MedHat_Surface(T	Well tops	MEDICINE_HAT (Well tops)	V=V0=Vint	V0: Constant	2965.97
Surface	BaseMEDHAT_Surf	Well tops	BASE_MEDICINE_HAT (Well tops)	V=V0=Vint	V0: Constant	3255.66
Surface	2WS_Surface(TWT)	Well tops	SECOND_WHITE_SPECKS (Well tops)	V=V0=Vint	V0: Constant	3406.88
Surface	BFS_Surface(TWT)	Well tops	BASE_FISH_SCALES (Well tops)	V=V0=Vint	V0: Constant	2691.78
Surface	BowIsland_Surface(	Well tops	BOW_ISLAND (Well tops)	V=V0=Vint	V0: Constant	1509.44
Surface	JoliFou_Surface(TW	Well tops	JOLI_FOU (Well tops)	V=V0=Vint	V0: Constant	4491.32
Surface	Mannville_Surface(	Well tops	MANNVILLE (Well tops)	V=V0=Vint	V0: Constant	7019.56

FIG. 35. The Velocity Modeling dialogue box, displaying each time surface to be modeled with the corresponding V0 constant (m/s) obtained from the TDR defined during the well-tie process.

The velocity modeling process using the time surface which is a resultant of subsurface horizon interpretation on two 3-D seismic volumes, and the V0 constant to calculate a depth. If modeled correctly, the formation well tops that were computed in time (well-tie process) and in depth (property model) should intersect the newly depth-converted surfaces. Figure 36 demonstrates the 4 km x 5 km geophysical model that has been converted to depth, with the formation well tops intersecting the surfaces.

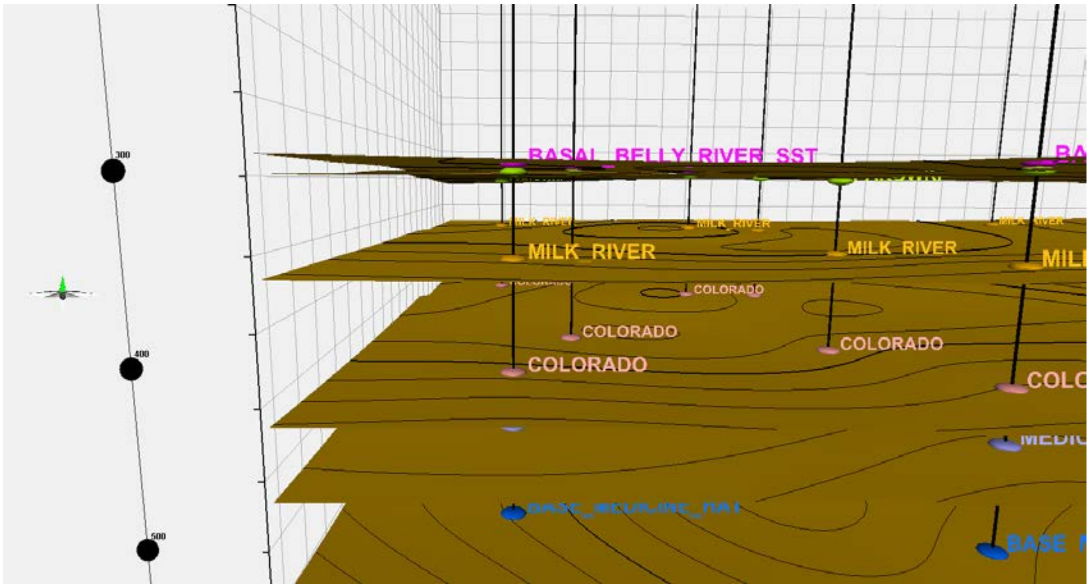

FIG. 36. The 4 km x 5 km geophysical model converted to depth by the velocity modeling process. Formation well tops displaying the surface name intersect the depth-converted surfaces at each respective well where a well-tie was computed.

With the geophysical model converted to depth, the surfaces were used to update the surfaces in depth for the 5 km^2 property model. A weight factor of 85% and 15% was used to determine the contribution from the geophysical and geological data, respectively. A larger weight factor was used on the geophysical data, as there was greater data density in the geophysical model with respect to subsurface horizon location.

1 km^2 Integrated Geostatic Model

The geostatic model that will be used for the CO_2 fluid simulation completed by the reservoir engineer will be a 1 km^2 clipped area of the integrated geophysical and geological model. This clipped region has been displayed on the maps provided in this report as a polygonal circle about the main well 7-22 on the GFRS site. The P10/50/90 framework used to identify the probability of conservative, typical, and optimistic effective porosity and permeability values will also be used for staging the time-lapse injection scenarios of the 1000 tons of CO_2.

CONCLUSIONS

A 5 km^2 geostatic model was developed in a 5 km radius about the main well 7-22 in the GFRS area in Newell County, Alberta. Existing wireline and 3-D seismic reflection data was used to interpret the subsurface horizons to a depth of 700 m (top of the Mannville Group). Structural maps of the primary and secondary target and seal intervals were constructed, demonstrating the elevation depth and displaying the topography of each formation top. Both isopach and isochron maps were created using the difference of surface thicknesses computed between two sequential surfaces.

The two main geological properties that were focused on to populate the 3-D model that were chosen include effective porosity and permeability. Using the limited core data analyses, a relationship between porosity and permeability was established for the target and seal intervals. Variogram analyses were completed for the two properties in each zone of the model. The properties were populated into the model by utilizing a Gaussian Random Function Simulation algorithm. To gain a better understanding of the uncertainty within the data, a P10/50/90 framework was used to characterize the conservative, typical, and optimistic ranges within the distribution of the effective porosity data in each target and seal interval.

A velocity model was constructed utilizing the time surfaces which included interpretation from both the TDR from the synthetic seismograms and well-ties, as well as the subsurface reflector interpretation on both the 1997 and 2014 3-D seismic volumes in the GFRS study area. Depth conversion involved using the produced velocity model, TDR, and velocity property modeling for each subsurface formation. The depth-converted geophysical model was integrated into the 5 km^2 property model to update the subsurface formation locations using a weighting factor of the different data sets.

A 1 km^2 clipped region of the 5 km^2 integrated geostatic model about the main 7-22 well for the two injection and corresponding seal intervals, which will be used for the CO_2 fluid simulation. From the P10/50/90 framework, the attributed pore volume realization assigned to each percentile will be further used in the simulation for the CO_2 injection.

Future work

Future work to be conducted on this model involves further characterization of the Medicine Hat Member sandstones. The current porosity and permeability predictions consider the entire interval from the Medicine Hat to the Base Medicine Hat formation top. Resistivity logs have been obtained and will be examined to find a cut-off to define the individual sand packages, as the contact is gradual and not sharp.

Once the individual sandstone packages have been isolated, porosity and permeability statistics will be completed using the P10/50/90 framework. The simulation of the CO_2 injection into the primary and secondary target intervals will follow. The simulation will be completed for all P10/50/90 realizations, which will take into consideration and act to test the validity of the modeled effective porosity and permeability properties. The simulation results will also be examined for P-wave and S-wave behaviour on the interfaces of the primary and secondary target intervals.

Other 2-D seismic reflection sections are available courtesy of Cenovus Energy, and will be incorporated to the model to enhance data density and interpretation of the subsurface horizons.

Lastly, to gain a greater understanding of the porosity and permeability distribution in the subsurface, a better relationship between total and effective porosity needs to be identified in order to create accurate permeability properties. This can be used once the injection well is drilled and cored, where the core data measurements are within the GFRS site and the two properties can be updated within the 5 km^2 integrated geostatic model.

ACKNOWLEDGEMENTS

I would like to thank Wade Zaluski (P. Geo – Schlumberger) for his expertise and knowledge of modeling that contributed to this project. As well, I would like to thank Valerie Smith (Reservoir Geophysicist – Schlumberger) for aiding in the velocity modeling process for domain conversion. I would also like to thank Dr. Per Pedersen for his constructive discussions on property modeling and geological background of the research area.

Thank you to Carbon Management Canada for providing the funding for this research to develop the Geoscience Field Research Site (GFRS) in Alberta and undertaking the new 3-D/3-C seismic survey. As well, we thank the sponsors of CREWES for their support. We also gratefully acknowledge support from NSERC (Natural Science and Engineering Research Council of Canada) through the grant CRDPJ 379744-08.

Thank you to Schlumberger Canada Limited for providing the Petrel™ E&P Software Platform, whose license was provided to the Department of Geoscience at the University of Calgary and was used for the development of the geostatic model.

Lastly, thank you to IHS Energy Canada for providing Accumap® and Acculog® software, whose license was provided to the Department of Geoscience at the University of Calgary and was used to obtain the extensive well data used in this project.

REFERENCES

Abbas, M.Y. (2009). Incorporating seismic attribute variation into the pre-well placement workflow: A case study from Ness County, Kansas, USA (Master's Thesis). Department of Geology, College of Arts and Sciences, Kansas State University.

Alshuhail, A. (2011). CO2 Sequestration Site Characterization and Time-lapse Monitoring Using Reflection Seismic Methods. Ph.D. Thesis, CREWES, University of Calgary.

Bachu, S. (2002). Sequestration of CO2 in Geological Media Criteria and Approach for Site Selection in Response to Climate Change. Energy Conversion and Management, vol. 43, pp. 87-102.

Barnes, R. (2014). Variogram Tutorial. Golden Software, Inc. Obtained on April 16, 2014 from http://www.goldensoftware.com/variogramTutorial.pdf.

Beaton, A. (2003). Coal-Bearing Formations and Coalbed-Methane Potential in the Alberta Plains and Foothills. Alberta Energy and Utilities Board/Alberta Geological Survey. CSEG Recorder, vol. 28(9). Obtained on October 19, 2014 from http://csegrecorder.com/articles/view/coal-bearing-formations-and-coalbed-methane-potential-in-the-alberta-plains.

Butch, R. (2014). Personal communication. Advanced petrophysicist at Schlumberger Canada Ltd.

Christopher, J., Yurkowski, M., Nicolas, M., and Bamburak, J. (2006). The Cenomanian-Santonian Colorado formations of eastern southern Saskatchewan and southwestern Manitoba; in Gilboy, C.F. and Whittaker, S.G. (eds.), Saskatchewan and Northern Plains Oil & Gas Symposium 2006, Saskatchewan Geological Society Special Publication 19, pp. 299-318. Obtained on April 15, 2014 from http://www.gov.mb.ca/iem/petroleum/pubcat/Christopher_et_al.pdf.

Esri. (2012). Key concepts of geostatistical simulation. ArcGIS Help 10.1, ArcGIS Resources. Obtained on April 16, 2014 from http://resources.arcgis.com/en/help/main/10.1/index.html#//003100000058000000.

Google, INEGI. (2014). Accessed September 2014 online from © Google Maps 2014.

Hamblin, A.P. and Abrahamson, B.W. (1993). Offlapping progradational cycles and gas pool distribution in the Upper Cretaceous "Basal Belly River" Sandstones, Judith River Group, Southern and Central Alberta. Open File 2672, Geological Survey of Canada.

Hamblin, A.P. and Abrahamson, B.W. (1996). Stratigraphic architecture of "Basal Belly River" cycles, Foremost Formation, Belly River Group, subsurface of southern Alberta and southwestern Saskatchewan. Bulletin of Canadian Petroleum Geology, vol. 44(4), pp. 654-673.

Hamblin, A.P. and Lee, P.J. (1995). Assessment of Upper Cretaceous-Tertiary gas resources, post-Colorado strata, WCSB, Interior Plains. Geological Survey of Canada, Open File 2058, pp. 335-336.

Hamblin, A.P. (1997). Regional Distribution and Dispersal of the Dinosaur Park Formation, Belly River Group, Surface and Subsurface of Southern Alberta. Bulletin of Canadian Petroleum Geology, vol. 45(3), pp. 377-399.

Hovorka, S.D., Choi, J.-W., Meckel, T.A, Trevino, R.H., Zeng, H., Kordi, M., Wang, F.P. (2008): Comparing carbon sequestration in an oil reservoir to sequestration in a brine formation- field study: presented at the 9th International Conference on Greenhouse Gas Control Technologies (GHGT-9), Washington, D.C., November 16-20, 2008. GCCC Digital Publication #08-03 D.

IPCC. (2005). IPCC Special Report on Carbon Dioxide Capture and Storage. Prepared by Working Group III of the Intergovernmental Panel on Climate Change. (B. Metz, O. Davidson, H. de Coninck, M. Loos, & L. Meyer, Eds.) Cambridge, United Kingdom and New York, NY, USA: Cambridge University Press.

Lawton, D.C. (2013). Geoscience Field Research Station Proposal Summary. Carbon Management Canada, University of Calgary in October, 2013.

Lawton, D.C., Adamson, R., and Osadetz, K. (2014). Carbon Management Canada: Containment and Monitoring Institute (CaMI). Presentation to the Alberta Energy Regulator, January 21, 2014.

Leckie, D.A. and Smith, D.G. (1992). Regional Setting, Evolution, and Depositional Cycles of the Western Canada Foreland Basin: Chapter 1. AAPG Special Volume 55: Foreland Bains and Fold Belts, pp. 9-46. Obtained online on April 15, 2014 from http://archives.datapages.com/data/specpubs/basinar3/data/a136/a136/0001/0000/0009.htm?q=%2BtitleStrip%3Awestern+titleStrip%3Agulf+titleStrip%3Amexico+Basin%3Atectonics+titleStrip%3Asedimentary+titleStrip%3Abasins+titleStrip%3Apetroleum+titleStrip%3Asystems.

Leckie, D.A., Bhattacharya, J.P., Bloch, J., Gilboy, C.F., and Norris, B. (2004). Chapter 20 – Cretaceous Colorado / Alberta Group of the Western Canada Sedimentary Basin. Alberta Geological Survey. Obtained online on April 15, 2014 from http://www.ags.gov.ab.ca/publications/SPE/PDF/SPE_004/low_res/chapter_20.pdf.

Leckie, D.A., Bhattacharya, J.P., Bloch, J., Gilboy, C.F., and Norris, B. (2012). Chapter 20: Cretaceous Colorado/Alberta Group of the Western Canada Sedimentary Basin. Obtained October 18, 2014 from http://www.ags.gov.ab.ca/publications/wcsb_atlas/a_ch20/ch_20.html#fir.

Leckie, D.A., Bhattacharya, J.P., Bloch, J., Gilboy, C.F., and Norris, B. (2013). Chapter 20: Cretaceous Colorado/Alberta Group of the Western Canada Sedimentary Basin. In: Geological Atlas of the Western Canada Sedimentary Basin. Alberta Geological Survey. Obtained August 26, 2014 from http://www.ags.gov.ab.ca/publications/wcsb_atlas/a_ch20/ch_20.html

Mao-Jones, J. (2012). Decision & Risk Analysis. The Merrick Consultancy. Obtained April 16, 2014 from http://www.merrick.com/merrickandcompany/media/Resources/Energy/Whitepapers/Merrick-Decision-Risk-Analysis-White-Paper.pdf?ext=.pdf.

McNeil, D.H. (1984). The eastern facies of the Cretaceous system in the Canadian Western Interior. CSPG Memoir: The Mesozoic of Middle North America, vol. 9, pp. 145-171. Obtained online on April 15, 2014 from http://archives.datapages.com/data/cspg_sp/data/009/009001/pdfs/145.pdf.

McNeil, D.H. and Caldwell, W.G.E. (1981). Cretaceous Rocks and their foraminifera in the Manitoba Escarpment. Geological Association of Canada, Special Paper 21, pp. 439.

Natural Resources Canada (NRCAN). (2014). Lithological Units: Bearpaw Formation. Obtained on January 27, 2014 from http://weblex.nrcan.gc.ca/html/000000/GSCC00053000966.html.

Natural Resources Canada (NRCAN). (2014). Lithological Units: Foremost Formation. Obtained on January 27, 2014 from http://weblex.nrcan.gc.ca/html/005000/GSCC00053005119.html.

Natural Resources Canada (NRCAN). (2014). Lithological Units: Oldman Formation. Obtained on January 27, 2014 from http://weblex.nrcan.gc.ca/html/011000/GSCC00053011229.html.

Nielsen, K.S. and Schroder-Adams, C.J. (1999). Upper Colorado Group lithology and wire line log correlation in southwestern Saskatchewan. In Summary of Investigations 1998, Saskatchewan Geological Survey, Saskatchewan Energy Mines, miscellaneous Report 98-4, pp. 79-84.

Nielsen, K.S., Schroder-Adams, C.J., and Leckie, D.A. (2003). A new stratigraphic framework for the Upper Colorado Group (Cretaceous) in southern Alberta and southwestern Saskatchewan, Canada. Bulletin of Canadian Petroleum Geology, vol. 51(3), pp. 204-246.

Nielsen, K.S., Schroder-Adams, C.J., Leckie, D.A., Haggart, J.W., and Elberdak, K. (2008). Turonian to Santonian paleoenvironmental changes in the Cretaceous Western Interior Sea: The Carlile and Niobrara formations in Southern Alberta and southwestern Saskatchewan, Canada. *Palaeogeography, Palaeoclimatology, Palaeoecology,* vol. 270, pp. 64-91.

Pedersen, P.K. (2013-4). Personal Communication. Associate Professor, Department of Geoscience. University of Calgary, 2500 University Dr. NW, Calgary, Alberta, T2N 1N4.

Rider, M. and Kennedy, M. (2011). The Geological Interpretation of Well Logs. 3rd Edition, published by Rider-French Consulting Ltd. Pp.132.

Robinson, C.C. (2008). A multidisciplinary approach to evaluating shale gas potential in a biogenic gas system; the upper Colorado Group shales in southeastern Alberta. MSc. Thesis, University of Calgary, Alberta, Canada.

Roca, X., Rylaarsdam, J.R., Zhang, H., Varban, B.L., Sisulak, C.F., Bastedo, K., and Guy Plint, A. (2009). An allostratigraphic correlation of Lower Colorado Group (Albian) and equivalent strata in Alberta and British Columbia, and Cenomanian rocks of the Upper Colorado Group in southern Alberta. Bulletin of CSPG, vol. 58(4): pp. 259-299. Obtained online on April 15, 2014 from http://archives.datapages.com/data/cspg/data/056/056004/pdfs/259.pdf.

Russel, L.S. and Landes, R.W. (1940). Geology of the southern Alberta Plains. Geological Survey of Canada, Memoir 221, pp. 223.

Schlumberger Limited Canada. (2014). Petrel E&P Software Platform. License used in the Department of Geosciences, University of Calgary, 844 Campus Place NW, Calgary, Alberta, T2N 1N4.

Schroder-Adams, C.J., Adams, P.J., Leckie, D.A., Bloch, J., Craig, J., and Seif El-Dein A.S. (1997). Upper Cretaceous Medicine Hat Formation and First White Speckled Shale in southeastern Alberta: evidence for localized shallow water deposition. Bulletin of Canadian Petroleum Geology, vol. 45(3): pp. 356-376

Shetsen, I. (1987). Quaternary Geology, Southern Alberta. Alberta Research Council. Map 207.

Smyth, R.C., Carr, D.L., Hovorka, S.D., Coleman, S., Breton, C.A., and Miller, E.N. (2011). Continued evaluation of potential for geologic storage of carbon dioxide in the southeastern United States: The University of Texas at Austin, Bureau of Economic Geology, pp. 39, GCCC Digital Publication Series #11-26.

Spangler, L. (2007). Measurement, Monitoring & Verification. Carbon Sequestration Leadership Forum. Obtained October 23, 2014 from http://www.cslforum.org/publications/documents/SpanglerMMVCSLFWorkshop050707.pdf.

Statios. (2004). Variograms. Geostatistical Software & Services. Obtained on April 16, 2014 from http://www.statios.com/Resources/04-variogram.pdf.

Staub, M., Galietti, B., Oxarango, L., Khire, V., and Gourc, J.P. (2009). Porosity and hydraulic conductivity of MSW using laboratory-scale tests. Third International Workshop “Hydro-Physico-Mechanics of Landfills”, Braunschwieg, Germany, 10-13 March 2009, Pp. 1-10.

Taylor, S.E. (2011). Shale Gas Potential of the Late Cretaceous Upper Colorado Group; Bigstick Pool, Southeastern Alberta and Southwestern Saskatchewan. Dissertation submitted to the Department of Geoscience, University of Calgary, Calgary, AB.

Thomas, L. (2002). Coal Geology. John Wiley & Sons. Obtained online on April 16, 2014 from http://books.google.ca/books?id=4oYWx90ybY8C&printsec=frontcover&source=gbs_ge_summary_r&cad=0#v=onepage&q&f=false.

Trautz, R.C., Pugh, J.D., Varadharajan, C., Zheng, L., Bianchi, M., Nico, P.S., Spycher, N.F., Newell, D.L., Esposito, R.A., Wu, Y., Dafflon, B., Hubbard, S.S., and Birkholzer, J.T. (2012). Effect of Dissolved CO2 on a Shallow Groundwater System: A Controlled Release Field Experiment. American Chemical Society. Environmental Science and Technology, vol. 47, pp. 298-305.

Wang, J. (2008). Integrated reservoir characterization and simulation studies in stripper oil and gas fields. Dissertation submitted to Texas A&M University for Doctor of Philosophy, Department of Petroleum Engineering.

Webb, A.C., Schroder-Adams, C.J., and Pedersen, P.K. (2005). Regional subsurface correlation of Albian sequences north of the Peace River in NE British Columbia: northward extent of sandstones of the Falher and Notikewin members along the eastern flank of the foredeep. Bulletin of Canadian Petroleum Geology, vol. 53, pp. 165-188.

WorleyParsons Komex. (2008). Regional Groundwater Resource Assessment for the County of Newell No. 4. Resources and Energy, Environment & Water Resources. County of Newell and AAFC-PFRA, pp. 1-105.

Yong, S. (2014). Personal Communication. Reservoir Engineer, Carbon Services. Schlumberger Canada Limited, 200 125-9th Avenue SE, Calgary, Alberta, T2G0P6.

Zahid, M. (2007). Basic Petrophysical Formulae. Obtained online on February 20, 2014 from www.carbonet.net/PETROPHYSICAL_FORMULAE.ppt.

Zaluski, W. (2014). Personal Communication. Senior Geologist, Carbon Services. Schlumberger Canada Limited, 200 125-9th Avenue SE, Calgary, Alberta, T2G0P6.